AFOSR-TR- 82-0262

(5)

SEMI-ANNUAL TECHNICAL REPORT
1 May 1981 – 31 October 1981

ARPA Order No.:	3291.30
Program Code:	1A10
Name of Contractor:	Califorinia Institute of Technology
Effective Date of Contract:	1 November 1981
Amount of Contract:	$169,942
Contract Number:	F49620-81-C-0008
Principal Investigators:	David G. Harkrider (213) 356-6910
	Donald V. Helmberger (213) 356-6910
Program Manager and Telephone Number	William J. Best (202) 767-5011
Short Title of Work:	Body and Surface Wave Modeling of Observed Seismic Events

The views and conclusions contained in this
document are those of the authors and should
not be interpreted as necessarily representing
the official policies, either expressed or
implied, of the Defense Advanced Research
Projects Agency or the U. S. Government.

DTIC
ELECTED
S APR 6 1982
D

Seismological Laboratory
Division of Geological and Planetary Sciences
California Institute of Technology
Pasadena, California 91125

82 04 06 114

REPORT DOCUMENTATION PAGE		READ INSTRUCTIONS BEFORE COMPLETING FORM
1. REPORT NUMBER AFOSR-TR- 82-0262	2. GOVT ACCESSION NO.	3. RECIPIENT'S CATALOG NUMBER
4. TITLE *(and Subtitle)* Body and Surface Wave Modeling of Observed Seismic Events		5. TYPE OF REPORT & PERIOD COVERED Semi-annual Technical Report 1 May 1981 - 31 October 1981
		6. PERFORMING ORG. REPORT NUMBER
7. AUTHOR(s) David G. Harkrider Donald V. Helmberger		8. CONTRACT OR GRANT NUMBER(s) F49620-81-C-0008
9. PERFORMING ORGANIZATION NAME AND ADDRESS California Institute of Technology Seismological Laboratory, 252-21 Pasadena, California 91125		10. PROGRAM ELEMENT, PROJECT, TASK AREA & WORK UNIT NUMBERS 61102F 2309/A1
11. CONTROLLING OFFICE NAME AND ADDRESS AFOSR/NP Building 410 Bolling AFB, D. C. 20332		12. REPORT DATE 1 May 1981 - 31 October 1981
		13. NUMBER OF PAGES 102
14. MONITORING AGENCY NAME & ADDRESS*(if different from Controlling Office)*		15. SECURITY CLASS. *(of this report)* Uncl
		15a. DECLASSIFICATION/DOWNGRADING SCHEDULE

16. DISTRIBUTION STATEMENT *(of this Report)*

Approved for public release; distribution unlimited

17. DISTRIBUTION STATEMENT *(of the abstract entered in Block 20, if different from Report)*

18. SUPPLEMENTARY NOTES

19. KEY WORDS *(Continue on reverse side if necessary and identify by block number)*

Representation theorum applications, laterally inhomogeneous source regions, Rayleigh wave excitation, mixed path corrections, region body wave source inversions, modeling irregular surfaces and spall, Kirchoff-Helmholtz scattering applications. → This research dealt with →

20. ABSTRACT *(Continue on reverse side if necessary and identify by block number)*

The research performed under the contract during the period 1 May through 31 October 1981 can be divided into three main topics, coupling of surface waves in laterally inhomogeneous source regions to teleseismic propagation paths, using regional waveforms to determine the source parameters of moderate-size earthquakes and the application of the Kirchoff-Helmholtz integral to seismic problems. First,

In Section II, the Representation Theorem (RT) is used to numerically

DD FORM 1473
1 JAN 73

cont

evaluate the effectiveness of two commonly used algorithsm for modeling Rayleigh wave propagation across lateral inhomogenities. Of the two, the conservation of lateral energy flux approximation most closely matches the maximum peak-to-peak amplitudes as seen through an LP-LRSM instrument. Another interesting result is that in using the RT to model seismic events, the short-periods are dominated by the displacement forcing functions and the long periods are controlled by the stress forcing functions. This is in agreement with other investigators in that they found that body waves were controlled by the displacement forcing functions and surface waves by the stress forcing functions.

Next,

In Section III, a procedure for the systematic determination of source parameters from regional body waves is presented. A least squares inversion based on a cross-correlation of the data and squares inversion based on a cross-correlation of the data and synthetics is used to determine the fault mechanisms of a profile of the $P_{n\ell}$ synthetics and five earthquakes. The synthetics are for a western U.S. model which seems to be more than adequate for most continental regions. Three of the earthquakes are in the western U.S. Two other earthquakes, one in Baffin Bay in the Arctic and the other in Turkey have been included to demonstrate that the Green's function are not unique to the U.S. Both dip-slip and strike-slip events are determined. It is shown that the inversion parameters are fairly insensitive to small changes in crustal thickness, P_n velocity and mean crustal velocity. The inversion precedure only requires a small data set and is particularly ideal for strike-slip earthquakes.

sub nl

A numerical method for evaluating the Kirchoff-Helmholtz integral with application to seismic problems is presented in Section IV. The method is applied to the calculation of reflections from mountains topography and the modeling of spall associated with nuclear events. For the latter, the calculations produce travel-time and amplitude anomalies consistent with observations from underground nuclear blasts.

Accession For	
NTIS GRA&I	☒
DTIC TAB	☐
Unannounced	☐
Justification	

By
Distribution/
Availability Codes

Dist	Avail and/or Special
A	

DTIC COPY INSPECTED 3

TABLE OF CONTENTS

I   SUMMARY

The research performed under the contract during the period 1 May through 31 October 1981 can be divided into three main topics, coupling of surface waves in laterally inhomogeneous source regions to teleseismic propagation paths, using regional waveforms to determine the source parameters of moderate-size earthquakes and the application of the Kirchoff-Helmholtz integral to seismic problems.

In Section II, the Representation Theorem (RT) is used to numerically evaluate the effectiveness of two commonly used algorithms for modeling Rayleigh wave propagation across lateral inhomogenities. Of the two, the conservation of lateral energy flux approximation most closely matches the maximum peak-to-peak amplitudes as seen through an LP-LRSM instrument. Another interesting result is that in using the RT to model seismic events, the short-periods are dominated by the displacement forcing functions and the long periods are controlled by the stress forcing functions. This is in agreement with other investigators in that they found that body waves were controlled by the displacement forcing functions and surface waves by the stress forcing functions.

In Section III, a procedure for the systematic determination of source parameters from regional body waves is presented. A least squares inversion based on a cross-correlation of the data and synthetics is used to determine the fault mechanisms of a profile of the $P_{n\ell}$ synthetics and five earthquakes. The synthetics are for a western U.S. model which seems to be more than adequate for most continental regions. Three of the earthquakes are in the western U.S. Two other

earthquakes, one in Baffin Bay in the Arctic and the other in Turkey have been included to demonstrate that the Green's functions are not unique to the U.S. Both dip-slip and strike-slip events are determined. It is shown that the inversion parameters are fairly insensitive to small changes in crustal thickness, P_n velocity and mean crustal velocity. The inversion precedure only requires a small data set and is particularly ideal for strike-slip earthquakes.

A numerical method for evaluating the Kirchoff-Helmholtz integral with application to seismic problems is presented in Section IV. The method is applied to the calculation of reflections from mountains topography and the modeling of spall associated with nuclear events. For the latter, the calculations produce travel-time and amplitude anomalies consistent with observations from underground nuclear blasts.

II

EVALUATION OF MIXED PATH RAYLEIGH WAVE TECHNIQUES USING THE

REPRESENATION THEOREM I. VERTICAL POINT-FORCE SOURCES.

by

Peter Glover and David G. Harkrider

INTRODUCTION.

In our semi-annual report for May 1981 we presented some preliminary results comparing a Representation Theorem approximation with two previously used analytical techniques for calculating Rayleigh waves generated by explosions in mixed-path media. The Representation Theorem method that we presented was approximate in that we used a whole space formulation for the forcing functions and coupled them to halfspace Green's functions. Thus the interactions of the P-waves generated by the explosion with the free surface within the source region and the contact between the paths were ignored. The discrepancies that we found between the Approximate Representation Theorem (ART) results and the two analytic methods, referred to as the Conservation of Lateral Energy Flux (CLEF) and Unit Transmission Coefficient (UTC) methods respectively, together with the large differences in amplitude between the CLEF and UTC results, indicated that we need to make the comparison of the two methods using the exact Representation Theorem (RT) results. To do this we require forcing functions for an explosion in a half-space which we propose to model using the finite-element code SWIS (Frazier and Petersen, 1974). However, based on our earlier work, we can currently compare the three

methods for a vertical point-force source. This paper makes this comparison. For the case where the source medium is Yucca Flat tuff and the propagation medium is CIT109 and including a vertical component LP LRSM instrument, we find that the CLEF method most closely matches the maximum peak-to-peak amplitude of the signal generated by the RT method. However, the phase distortion inherent in the CLEF method reduces the period associated with the maximum amplitude.

REPRESENTATION THEOREM VALIDATIONS.

The theoretical developement of the Representation Theorem method for calculating fundamental mode Rayleigh waves from complex sources has been developed in a series of papers and presentations (e.g. Harkrider et al., 1979; Apsel et al., 1980; Harkrider, 1981; and Glover and Harkrider, 1981a, b). Basically the method consists of surrounding the source by a closed surface $\sum_{SES}$ over which the stresses and displacements generated by the interaction of the source with the source region medium can be monitored. These quantities, which we refer to as forcing functions, are then convolved with the appropriate Green's functions for the exterior, or propagation medium. Details of this proceedure and corresponding equations can be found in the references. As we have previously pointed out, the RT method permits the convenient extension of detailed calculations of complex source/structure interactions to distances at which meaningful estimates of M_s can be made.

Harkrider (1981) presented some preliminary results in which we

compared the surface wave generated by a buried vertical point-force in a homogenous halfspace evaluated using the RT method with that calculated from the analytic formulation of Harkrider (1964, 1970). The results in both cases were somewhat "saw-toothed" due to problems associated with picking the origin time of the synthetic time series. We have since improved our numerical techniques for evaluating the Green's functions and eliminated this problem. Before we evaluate the mixed path techniques, we will show these new results in order to establish the accuracy of the RT method.

Figure 1 shows the geometry for the homogenous halfspace run. $\sum_{SES}$ is a cylinder of revolution with height and radius 2.1km. There are 11 nodes per side with a spacing of 0.2km (the corner node's contribution is evaluated twice). The source is placed at 0.4km depth. The forcing functions are then evaluated at each node using the finite element code SWIS (Frazier and Petersen, 1974). Figure 2 shows the contribution to the final solution for the sum of the nodes on the bottom and the side of $\sum_{SES}$, identified by forcing function component, whereas Figure 3 shows the corresponding sums for all the nodes. The total RT result is also shown in Figure 3 together with the analytic (Direct) result. All time series are sampled at 5 samples/sec and a cosine taper has been applied over the entire spectrum. The amplitude of the RT result is 91% of the Direct result, and the contributions from the stresses and displacements are approximately equal. However, when the results are convolved with a vertical component LP LRSM seismometer response (Figures 4 and 5) the final RT solution is dominated by the contribution from the stresses, specifically the normal stress on the bottom and the

tangential stress on the side in the approximate ratio 2:1.

The material properties of the homogenous halfspace run (Figure 1) are almost identical to those of the upper 14km of the layered model CIT109 (Table 1). Therefore we can use the forcing functions from the former with the Green's functions from the latter without introducing any appreciable error. Figures 6 and 7 show the corresponding results, again for a LP LRSM instrument, sampled at 5 samples/sec, but at 1200 km epicentral distance and without any tapering. In this case the peak-to-peak amplitude of the RT result is 97% of the amplitude of the direct result and the associated period of 13.6 sec is identical in both cases. For the dispersed signal, the final result is clearly dominated by the contribution from the vertical component of stress acting on the bottom and side of the cannister.

ANALYTIC APPROXIMATIONS.

The first of the analytic approximations that we compare using the RT method is the CLEF method applied by Bache et al. (1978) in an analysis of NTS events recorded at Tuscon, Arizona and Albuquerque, New Mexico. In Harkrider's notation, the frequency domain vertical component response to a point force in the mixed media may be written as

$$\{\overline{w}_o\} = -i\ \frac{\overline{F}(\omega)}{2}\ \left[\frac{w_s(D)}{w_o}\right]\ \left(\frac{C_r}{C_s}\right)^{1/2} \left(\underline{A}_{RS}\ \underline{A}_{Rr}\right)^{1/2} H_0^{(2)}(k_r r)$$

The second method is that used by Alexander et al. (1976) in an

analysis of a sequence of earthquakes at Oroville, California recorded at the SRO station at Albuquerque. The vertical component for this approximation is given by

$$\{\overline{w}_o\} = -i \ \frac{\overline{F}(\omega)}{2} \ \left[\frac{w_s \ (D)}{w_o} \right] \ \underline{A}_{Rr} \ H_o^{(2)}(k_r \ r)$$

where the subscript s and r denote properties of the source and propagation median respectively. These expressions can be evaluated using slight modifications of computer codes used to calculate the Direct results shown in Figures 5 and 7 with little appreciable increase in cost.

MIXED PATH CALCULATIONS.

With a minor modification of the finite element mesh, we can examine the Rayleigh waves from a point-force in a medium that differs from that of the receiver. Figure 8 shows the geometry for the runs that we made where the receiver was in the same homogenous propagation medium as in Figure 1. The source region medium was a cylinder with a height and radius of 1.8km with material properties of either Yucca Flat tuff or Climax Stock granite (Table 1). By keeping the position of $\sum_{SES}$ fixed, we were able to monitor the first 6 sec of energy transmitted across the impedance boundary.

Figure 9 shows the results for the two source media typical of NTS. For the Climax Stock case the rigidity ratio is approximately 0.6 and

the waveforms given by the three methods are similar. However the difference in amplitudes is significant. For the Yucca Flat case, where the rigidity ratio is approximately 0.1, the waveforms from the three methods are quite dissimilar and the amplitude variation is large. Both analytic results broaden the signal width compared to the RT result, indicating some phase distortion. When the traces are convolved with the response of a LP LRSM instrument (Figure 10), the differences between results of the three computational methods are noticeably reduced. For Climax Stock, the amplitudes given by the CLEF and UTC method are identical, though still somewhat larger than the RT result. For Yucca Flat , the amplitude disparities between the three methods are considerably less. The CLEF result shows some differences with respect to the RT result at the higher frequencies, but not so great as the UTC result which is dominated by high frequency energy.

We also convolved the Climax Stock forcing functions with the CIT109 Green's functions for a vertical component LP LRSM intsrument at 1200km. Figure 11 shows the RT method result together with the analytic results. The peak-to-peak amplitudes of the RT and CLEF results closely agree. The associated periods are 15 sec and 12 sec respectively. The UTC method gives amplitudes a factor of 3 too large at periods around 6 sec and these distort the signal. The amplitude of the 13 sec period is approximately equal to that given by the other methods.

It is interesting to note that the peak-to-peak amplitude of the mixed path result computed using the RT method is 4.0×10^{-21} cm compared to 3.6×10^{-21} cm for the pure CIT109 result. The source in both instances had a strength of 1 dyne.

DISCUSSION.

There are two main conclusions that can be drawn from these results. These are:

i) In order to compute the RT result it is only necessary to perform the convolutions using the vertical component of stress on $\sum_{SES}$ when the result is to be put through a LP LRSM instrument in order to compute an M_s. This should effect a considerable saving in computational effort when evaluating both forcing and Green's functions.

ii) that for the type of mixed paths considered here, and when seen through a LP LRSM instrument, the CLEF method gives results comparable to the RT method.

In light of these results, we are undertaking a similar analysis using a finite element simulation of an explosion source in a half space to generate forcing functions.

REFERENCES

Alexander, S. S., R. W. Tifft, and P. Glover, Comparison of earthquake source mechanisms for foreshock, mainshock, and aftershock sequences using Seismic Research Observatory (SRO) data, EOS, 57(12), p. 954, 1976.

Apsel, R., G. Rawson, G. Frazier, J. Fried, J. Sweet, and P. Glover, Near-source phenomena and their manifestations on signatures of more distant radiation of seismic energy, Del Mar Technical Associates Report DELTA-R-79-0042, 1980.

Bache, T. C., W. L. Rodi, and B. F. Mason, Source amplitudes of NTS explosions inferred from Rayleigh waves at Albuquerque and Tuscon, Systems, Science and Software Topical Report SSS-R-78-3690, 1978.

Frazier, G. A., and C. M. Petersen, 3-D stress wave code for the ILLIAC IV, Systems, Science and Software Report SSS-R-74-2103, 1974.

Glover, P., and D. G. Harkrider, Evolution of the mixed path Rayleigh techniques using the representation theorem, in Seismic wave propagation and source characterization symposium (Proc., Defense Advanced Research Projects Agency Rept., DARPA-NMR-81-03, Arlington, Va., 1981a.

Glover, P., and D. G. Harkrider, Evaluation of mixed path Rayleigh techniques using the representation theorem, EOS, 62, p. 947, 1981b.

Harkrider, D. G., Surface waves in multilayered media I. Rayleigh and Love waves from buried sources in a multilayered elastic half-space, Bull. Seismol. Soc. Am., 54, pp. 627-679, 1964.

Harkrider, D. G., Surface waves in multilayered media II. Higher mode spectra and spectral ratios from point sources in plane-layered earth models, Bull. Seismol. Soc. Am., 60, pp. 1937-1987, 1970.

Harkrider, D. G., P. Glover, G. A. Frazier, R. J. Apsel, and G. Fried, A method for propagating surface waves from complex seismic source regions to teleseismic distances, Earthquake Notes, 50(4), p. 29, 1979.

Harkrider, D. G., Coupling near source phenomena into surface wave generation; Identification of Seismic Sources - Earthquake or Underground Explosion, ed. E. S. Husebye and S. Mykkeltveit, D. Reidel Publishing Co., Boston, pp. 277-326, 1981.

Figure Captions

Figure 1. Run geometry for a vertical point force(s) in a homogeneous half-space. X's denote nodes on $\sum_{SES}$ at which forcing functions are calculated.

Figure 2. Contributions from sum of modes on bottom and side of $\sum_{SES}$, identified by forcing function component, for problem shown in Figure 1. Amplitudes are ground displacement in cm x 10^{-15} due to force of 1 dyne.

Figure 3. Total contributions, R. T. and Direct solutions. Units as in Figure 2.

Figure 4. Results as in Figure 2, but convolved with LPZ LRSM response, plotted on common scale.

Figure 5. Results of Figure 3 after convolution with LPZ LRSM instrument response.

Figure 6. Contributions from bottom and side of $\sum_{SES}$ for vertical point force of 1 dyne in model CIT109, convolved with LPZ LRSM instrument of 1200 km distance. Units are cm x 10^{-15}.

Figure 7. Total contribution, RT and Direct solutions for model CIT109.

Figure 8. Geometry for mixed-path runs shown in Figures 9 and 10. For Figure 11, receiver R was placed at $\Delta = 1200$ km.

Figure 9.   Comparison of the mixed-path results for 2 NTS source media, scale factors shown separately.

Figure 10.   Results of Figure 9 convolved with LPZ LRSM response.

Figure 11.   Mixed-path results for model CIT109, LPZ LRSM instrument included.
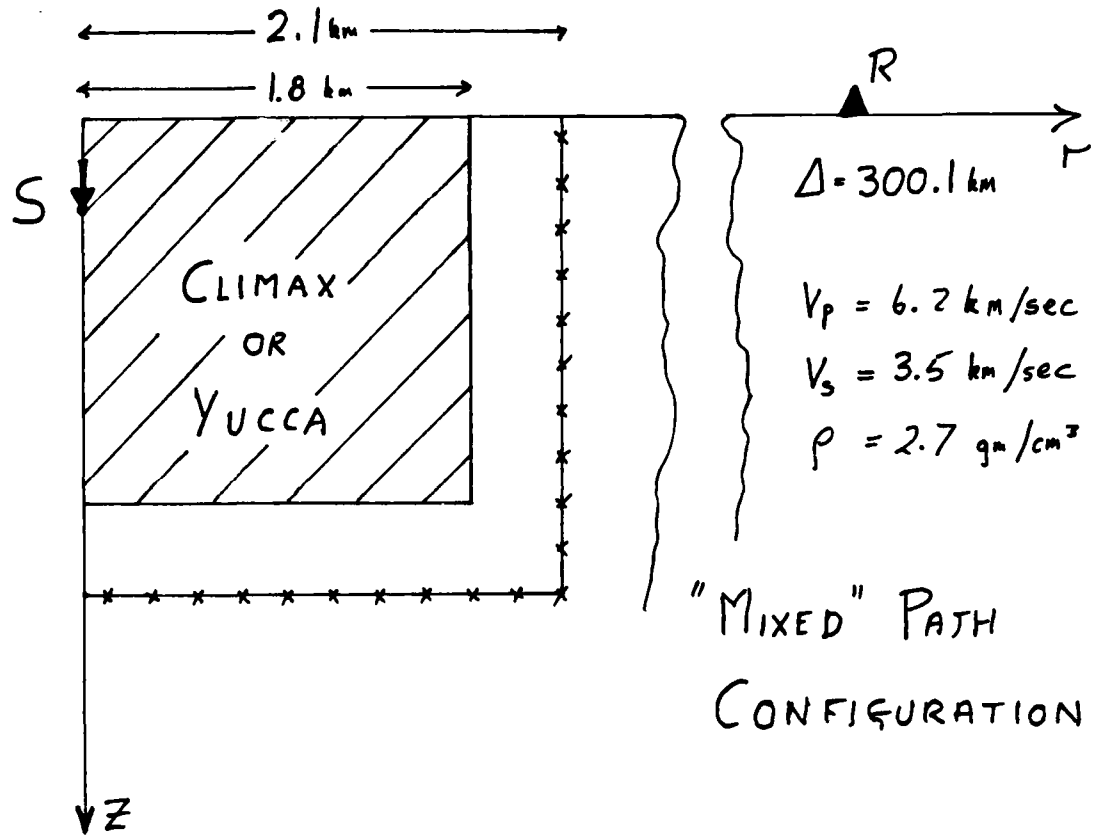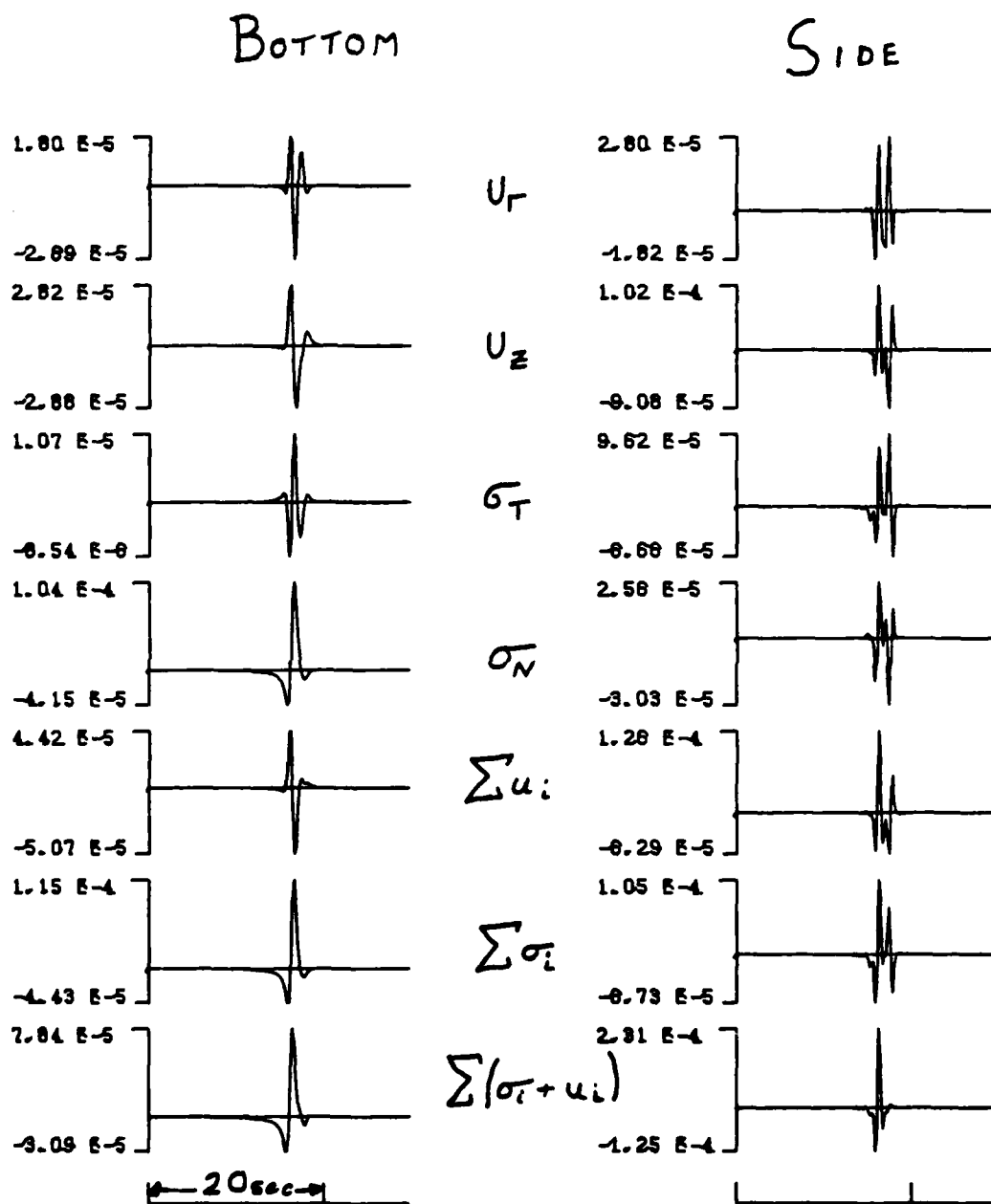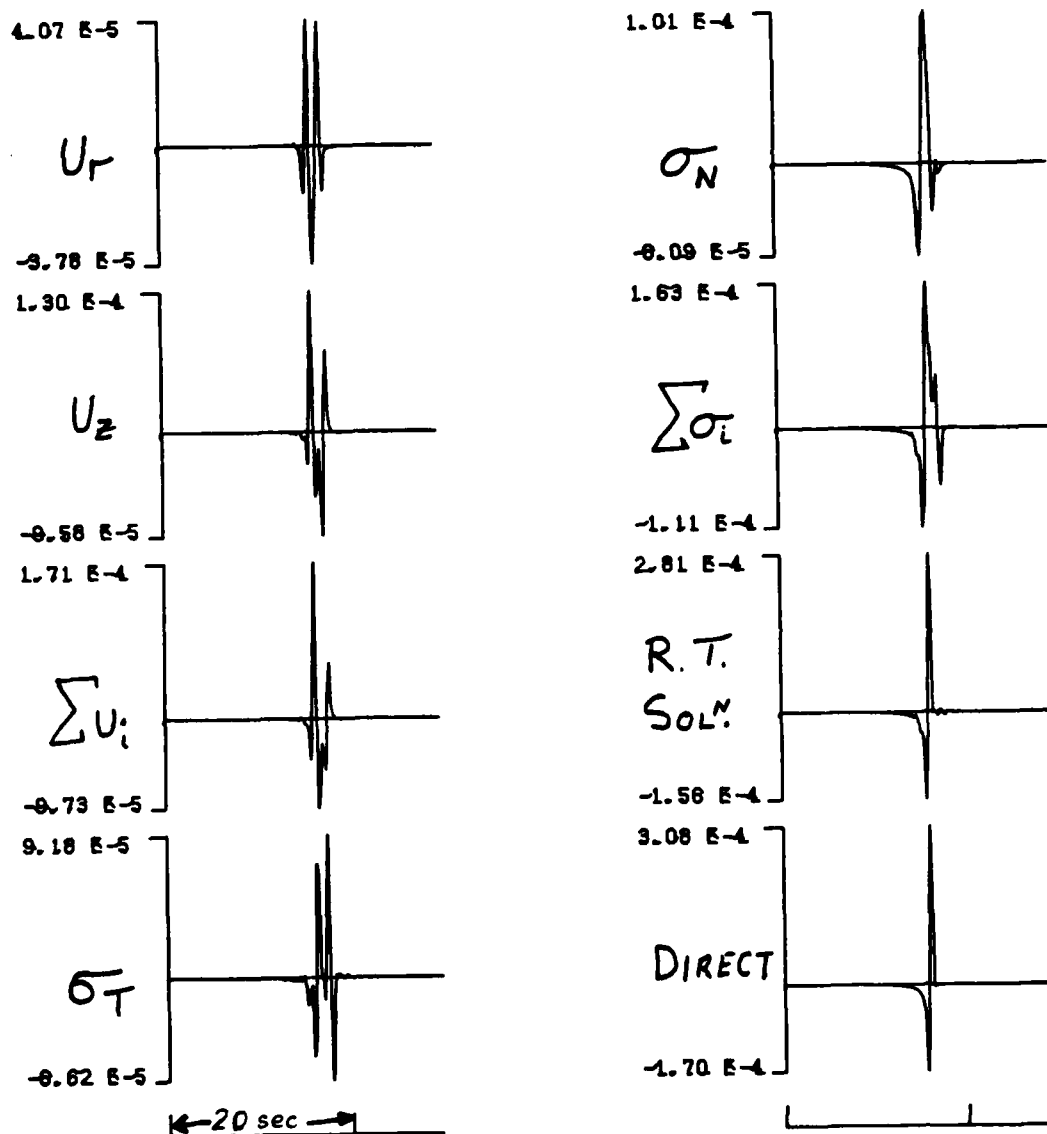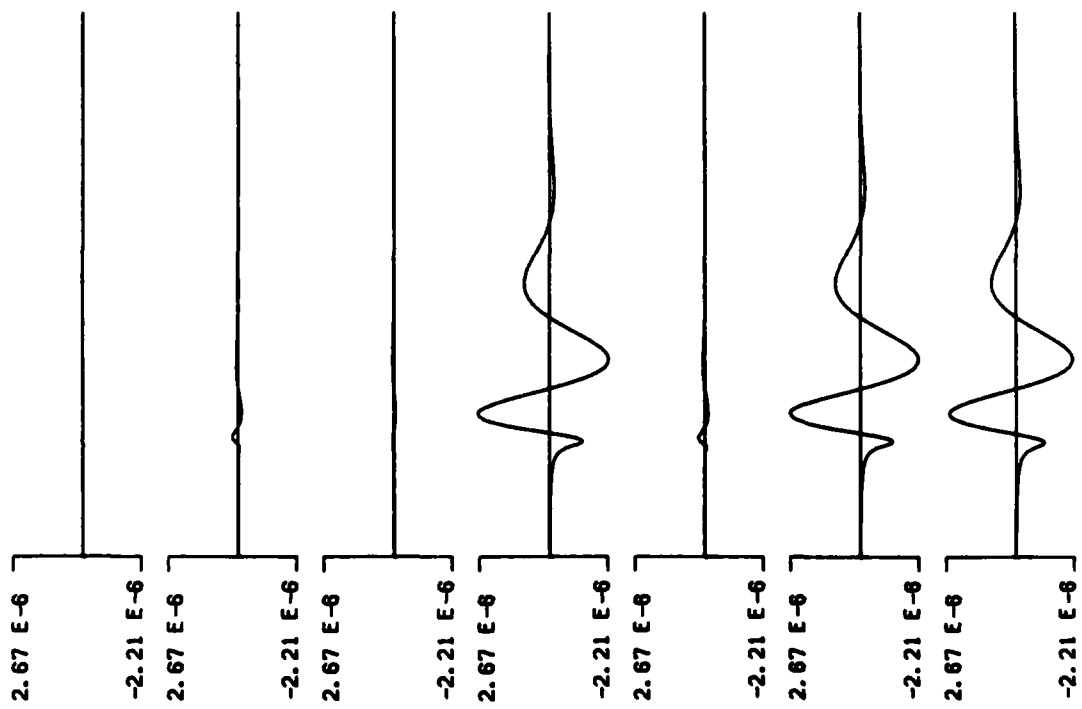
Figure 1

BOTTOM   SIDE

	Bottom		Side
1.80 E-5 / -2.89 E-5		U_r	2.80 E-5 / -1.82 E-5
2.82 E-5 / -2.88 E-5		U_z	1.02 E-4 / -9.08 E-5
1.07 E-5 / -6.54 E-8		σ_T	9.62 E-5 / -6.68 E-5
1.04 E-4 / -4.15 E-5		σ_N	2.58 E-5 / -3.03 E-5
4.42 E-5 / -5.07 E-5		$\sum u_i$	1.28 E-4 / -8.29 E-5
1.15 E-4 / -4.43 E-5		$\sum \sigma_i$	1.05 E-4 / -8.73 E-5
7.84 E-5 / -3.08 E-5		$\sum(\sigma_i + u_i)$	2.81 E-4 / -1.25 E-4

$\longmapsto 20\,\text{sec} \longrightarrow$

Figure 2

Figure 3

Figure 4

Figure 5

U_r

U_z

σ_T

σ_N

$\sum u_i$

$\sum \sigma_i$
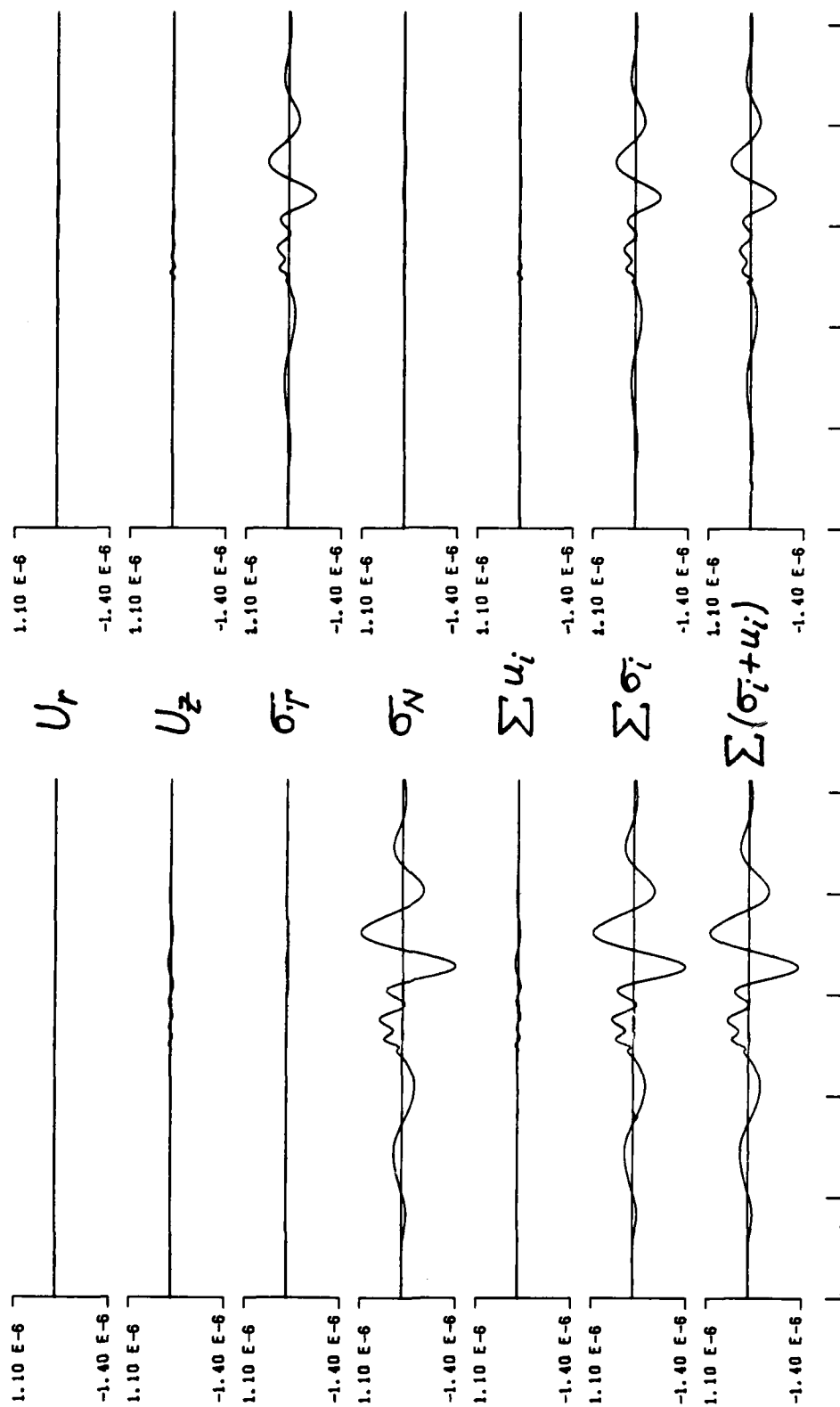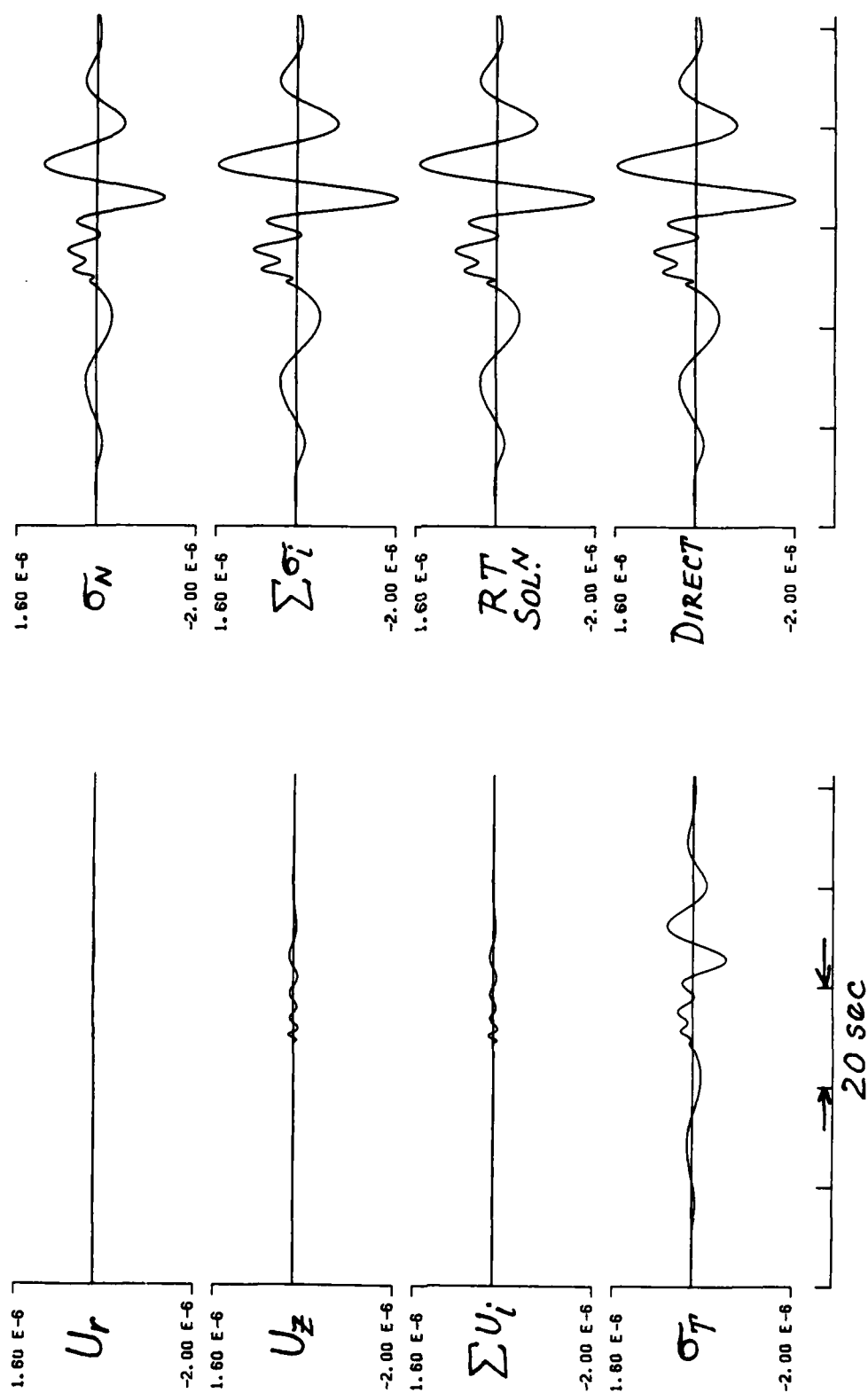
$\sum (\sigma_i + u_i)$

1.10 E-6

-1.40 E-6
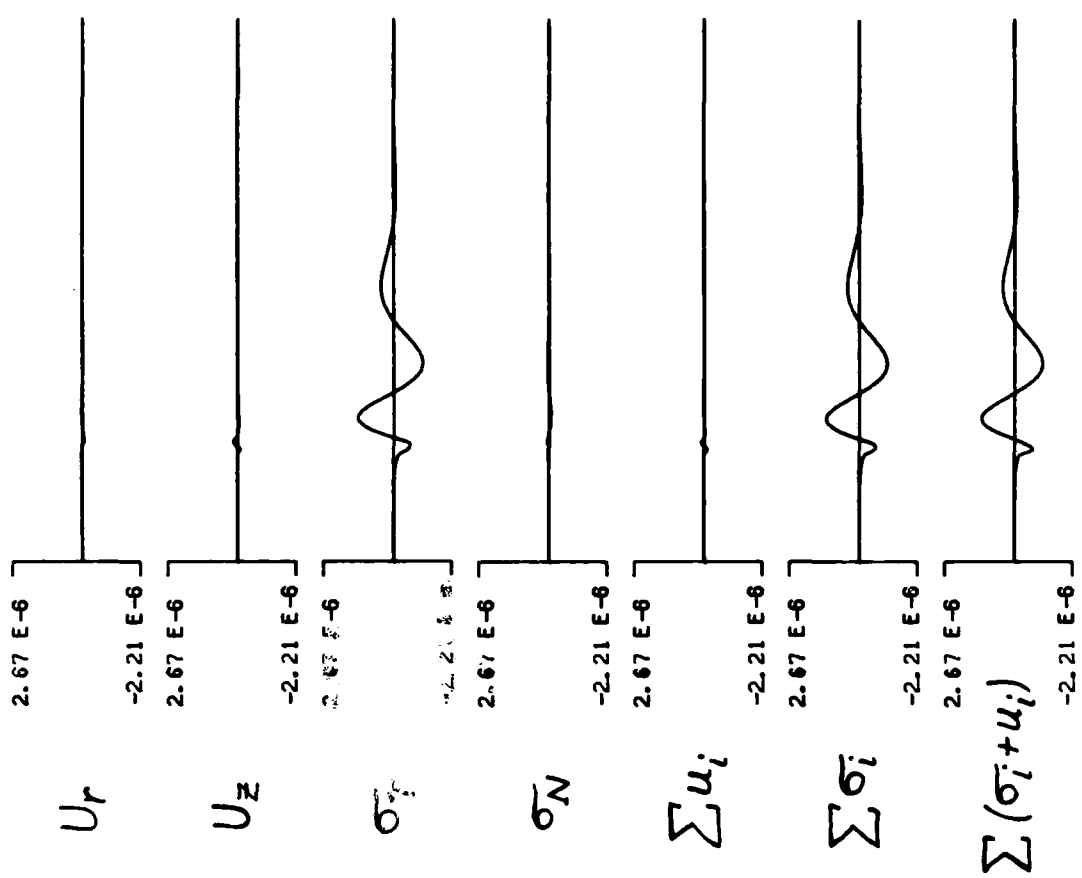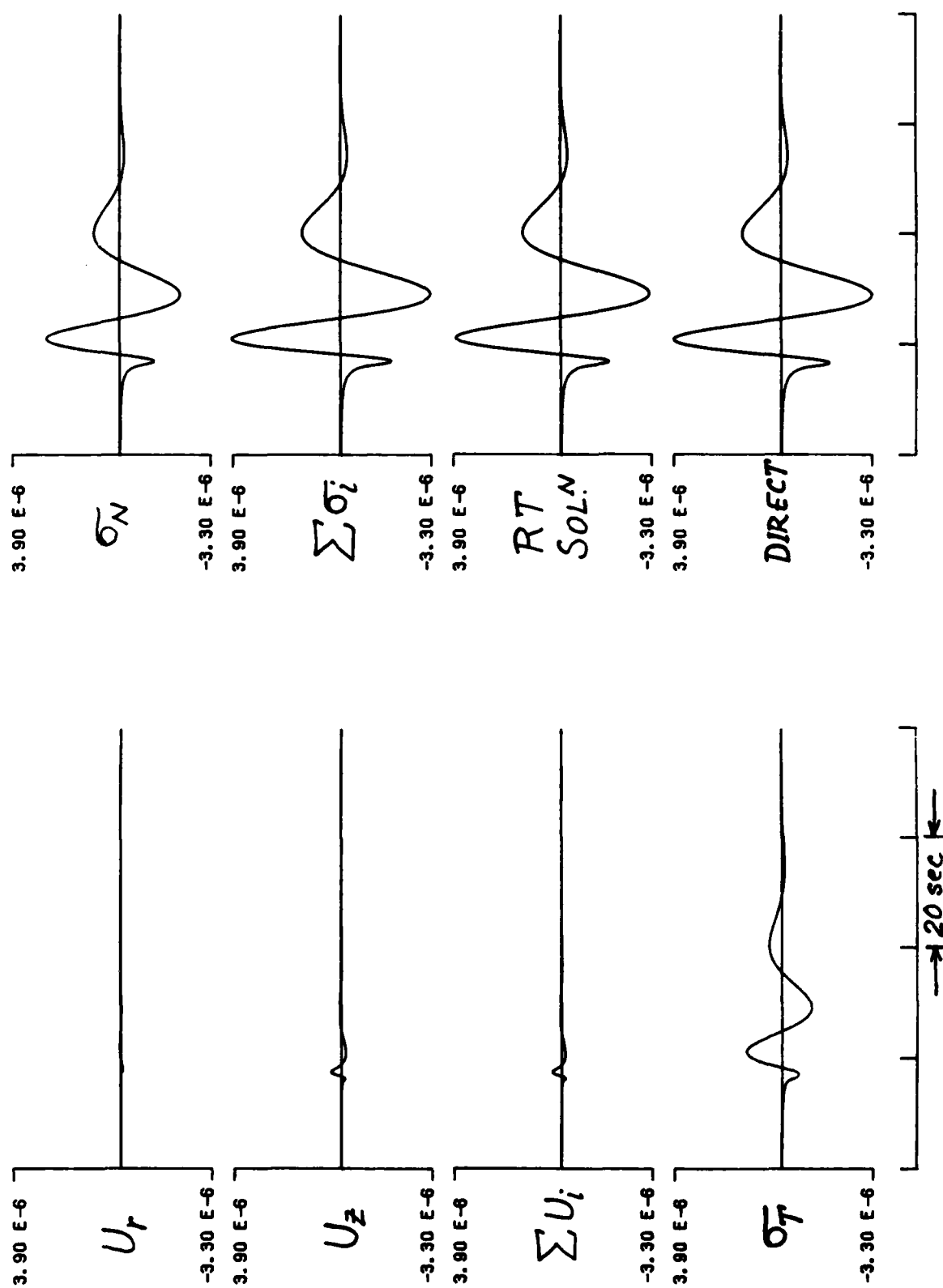
Figure 6

Figure 7

Configuration of Σ_{SES} for Buried Vertical Point Force

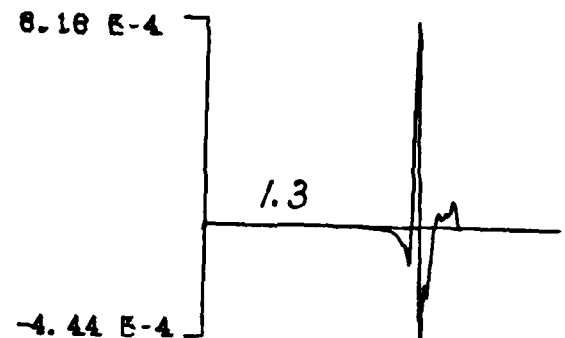

$\Delta = 300.1\,km$

$V_P = 6.2\ km/sec$

$V_S = 3.5\ km/sec$

$\rho = 2.7\ km/sec$
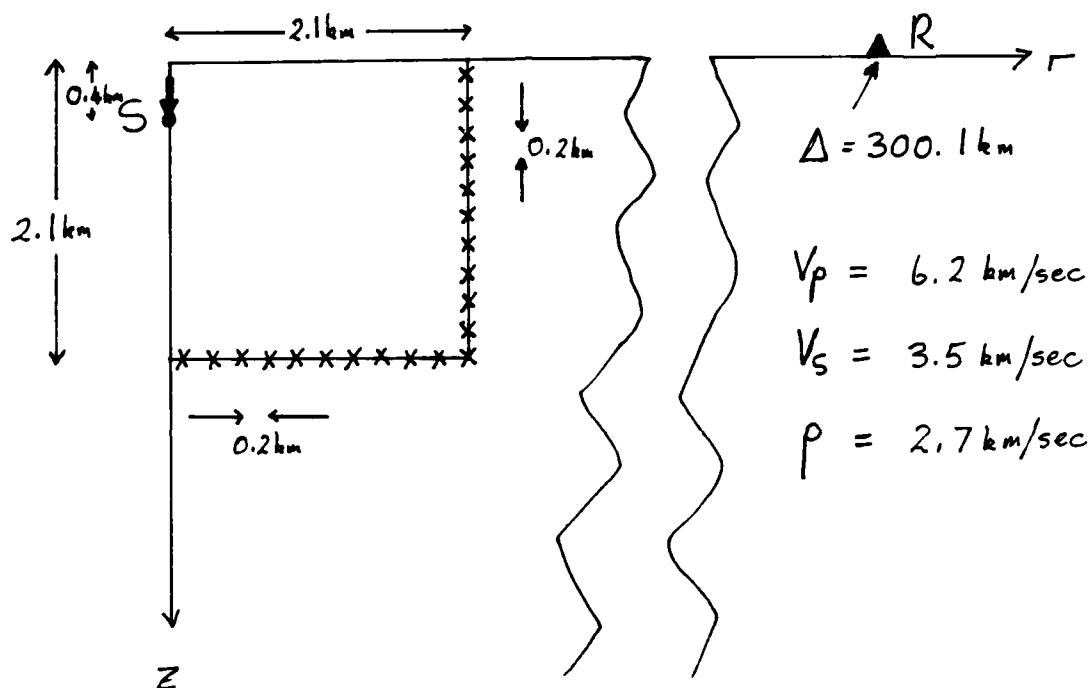
Figure 8

CLIMAX STOCK

YUCCA FLAT

4.38 E-4

6.3

RT

-1.92 E-4

8.18 E-4

1.3

-4.44 E-4

4.98 E-4

7.3

CLEF

-2.88 E-4

2.15 E-3

3.1

-9.38 E-4

8.48 E-4

9.8

UTC

-3.82 E-4

7.78 E-3

10.6

-2.83 E-3

|← 20 sec →|

$x\,10^{-19}\,cm$

$x\,10^{-18}\,cm$

Figure 9

Figure 10

2.04 E-6

RT

-1.94 E-6

1.96 E-6

CLEF

-2.24 E-6

7.14 E-6

UTC

-6.78 E-6

→| 20 sec |←
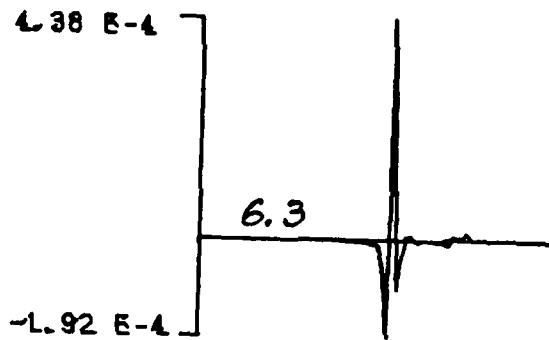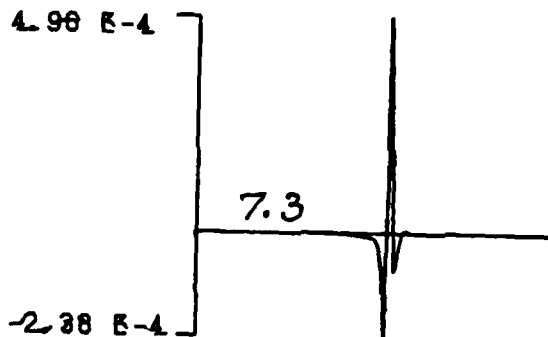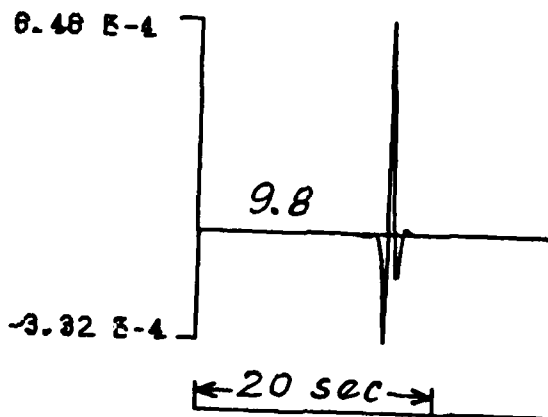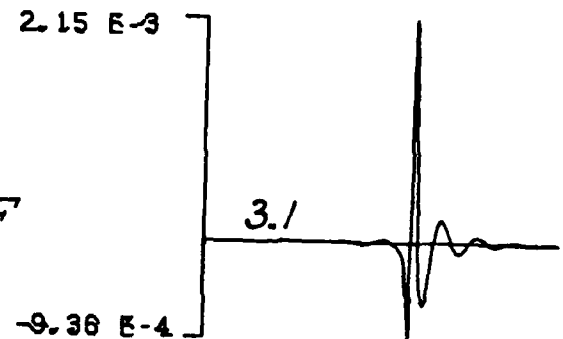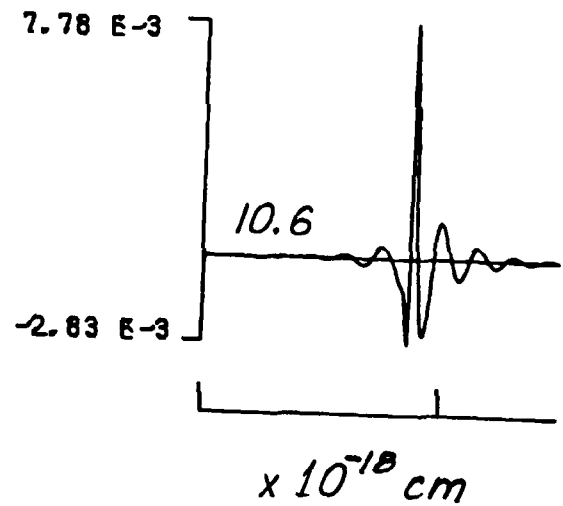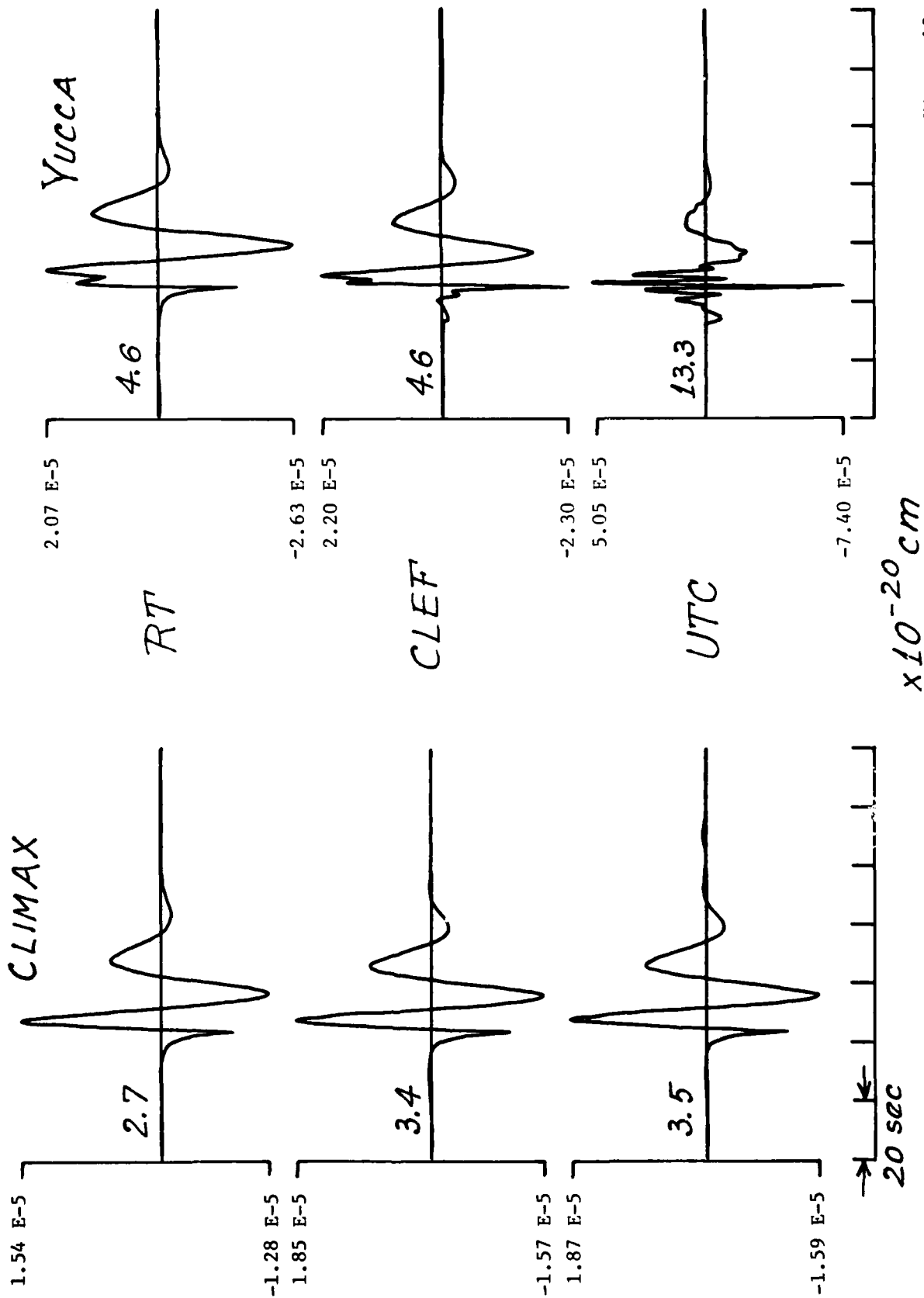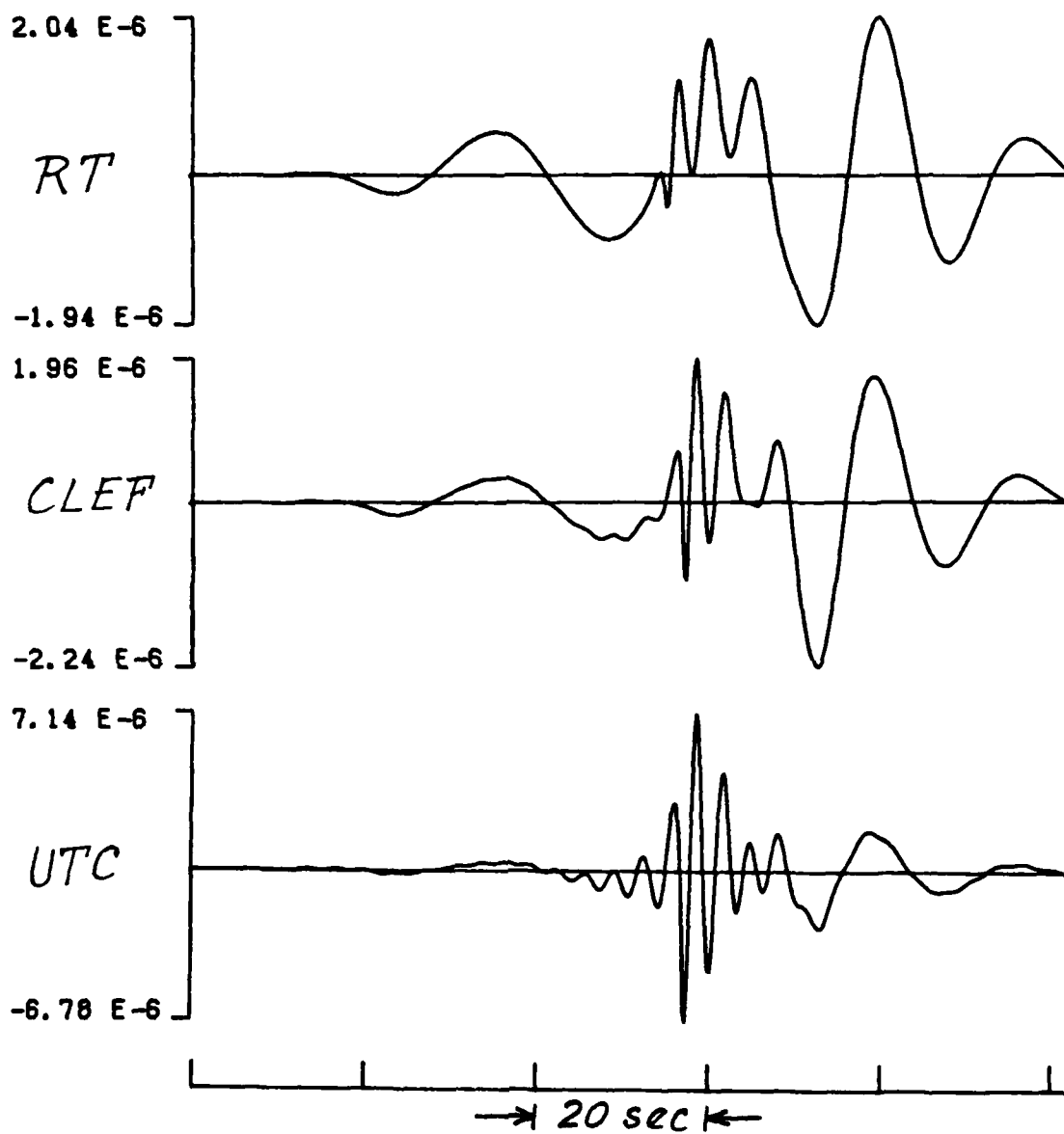
Figure 11

III

DETERMINING SOURCE PARAMETERS OF MODERATE-SIZE

EARTHQUAKES FROM REGIONAL WAVEFORMS

by

Terry C. Wallace

Don V. Helmberger

Seismological Laboratory
California Institute of Technology
Pasadena, California 91125

ABSTRACT

Waveform modeling of teleseismic long-period body wave phases of shallow earthquakes has proven quite effective in determining source parameters for events larger than magnitude six. Unfortunately, these teleseismic phases become too weak for the smaller events and regional data mudt be used which are generally much more complicated. This is because the crust-mantle system is acting like a leaky waveguide and a large number of rays are required to model the observations. In this report we review a procedure for the systematic determination of source parameters from the regional body waves. A least-squares inversion technique which is based on a cross-correlation of the data and a synthetic is used. The synthetics are a linear combination of the three fundamental faults. A set of profiles of the synthetics is presented. Although the synthetics are generated for a model developed for the western U.S., this model seems to be adequate for most continental regions. The inversion is parameterized in terms of fault strike, dip and rake; these parameters are relatively insensitive to small changes in crustal structure. Several examples are presented.

INTRODUCTION

A considerable amount of effort has been expended to determine the source parameters of moderate size earthquakes, although it can be besieged with difficulties. Ideally, a large amount of information can be derived from modeling the long-period body waves (see Helmberger, 1974; Langston and Helmberger, 1975). Unfortunately, if the earthquake is too small to be well recorded teleseismically, which is the case for many events in the magnitude range between 5 and 6, the fault plane orientation must be constrained by local short-period data and the seismic moment usually can not be determined unambiguously. The World-Wide Standard Seismograph Network (WWSSN) supplemented by other long-period stations and arrays provides sufficiently dense coverage in that most moderate size earthquakes occurring in continental regions will produce some on-scale records of the long-period body waves at regional distances. In the regional distance range (1 -12°) the wave guide properties of the crust produce complicated body wave signals; however, in most cases the long-period waveform is quite distinctive and sufficiently insensitive to crustal structure details to allow the separation of the source and structural information.

In this paper we review a procedure for extracting the source parameters of moderate size earthquakes from long-period regional phases. The technique involves an iterative inversion process which minimizes the difference between a synthetic seismogram and the observation. The synthetics are constructed using Green's functions computed for a single, very simple structure. These Green's functions appear to be an adequate model for most continental regions, thus allowing a quick and approximate determination of the fault parameters.

The inversion is parameterized in terms of strike dip and rake. The number of inversion parameters has been minimized so that inadequacies in the Green's functions are not over emphasised. Obviously, the structural model is more appropiate for certain region than others, so the inversion parameters chosen are those which are most robust. The main advantage of this technique is that it only requires a small data set. The general usefulness of this technique is illustrated by inverting regional data from earthquakes occurring in the United States, northern Canada and southern Europe.

THE GREEN'S FUNCTIONS

The techniques for constructing the Green's functions are discussed in detail elsewhere (Helmberger and Engen, 1980; Wallace et al., 1981). What is discussed here is some simplifying approximations and their applicability. The waveform of interest is that part of a regional seismogram which arrives before the S-wave. This waveform is referred to as $P_{n\ell}$. It is simplest to discuss $P_{n\ell}$ in terms of rays which are in a waveguide. The first part of $P_{n\ell}$ is dominated by P-waves (Pn) and, moving back into the record, the waveform contains progessively more SV (PL) contributions. The SV energy corresponds to rays which are reflected within in the crust and undergo subsequent mode changes at the free surface and the Moho. The interference of all the rays gives rise to the waveform; parameters such as crustal thickness or velocity contrast between the crust and Moho control the waveform dispersion. Figure 1 shows some typical $P_{n\ell}$ waveforms.

The Green's functions are constructed by summing generalized rays for a point shear dislocation. As an example, consider the following

equation for the vertical displacement in cylindrical coordinates:

$$w(r,z,\theta,t) = \frac{M_o}{4\pi\rho} \left(\dot{D}(t) * \sum_{i=1}^{3} W_i(t) A_i \right) \qquad (1)$$

where $\dot{D}(t)$ is the far field time history, ρ the source region density and M_o is the seismic moment. The summation process adds the contributions of the three fundamental faults; the W_i are the Green's functions for vertical strike-slip, vertical dip-slip and 45° dip-slip step dislocations respectively. The A_i are coefficients determined by source orientation and are given by:

$$A_1 (\theta,\lambda,\delta) = \sin 2\theta \cos \lambda \sin \delta + 1/2 \cos 2\theta \sin \lambda \sin 2\delta$$

$$A_2 (\theta,\lambda,\delta) = \cos \theta \cos \lambda \cos \delta - \sin \theta \sin \lambda \cos 2\delta \qquad (2)$$

$$A_3 (\theta,\lambda,\delta) = (1/2) \sin \lambda \sin 2\delta$$

where θ is the receiver azimuth from the end of the fault plane, λ is the rake angle and δ is the dip angle. The total displacement is then the sum of the displacements from each ray. The number of rays which are used is determined by the structure and the pass band of the observation. In our previous work we have shown that a single layer, corresponding to the crust, over a halfspace mantle is a sufficient structural model for regional long-period records to allow the extraction of source parameters of moderate size earthquakes.

As an example, Figure 2 shows a comparison of the synthetics and the records of the 1966 Truckee, California earthquake (which will be discussed in more detail). The synthetics were constructed from Green's functions computed for the crustal model in Table 1 and the fault orientation was determined by the inversion of the regional data. In this case the source time function and moment were determined by other

methods so that the synthetic amplitudes can be viewed as predictions. The numbers on the traces are maximum peak to peak amplitudes. The only noticeable difference between the data and the synthetics is the high frequency content which could be caused by several things; (1) the effects of attenuation within the crust have not been added to the synthetics, and (2) the very sharp boundaries in our model are efficient in trapping short-period energy. Overall, the fit of the synthetics to the data justifies the use of the simple model, and the high frequency content of the synthetics does not effect our ability to determine the source parameters.

The only expensive or complicated part of this modeling process is the actual generation of the Green's functions. For this reason, Figures 3 and 4, which give profiles of the vertical and radial responses for the three fundamental faults are presented. Most earthquakes which produce an on-scale $P_{n\ell}$ at long-period WWSSN stations have similar time functions (which is simply a reflection of the event size). In Figures 3 and 4 a trapezoid with a 1 second rise, 1 second top and 1 second fall is used for the far-field time history. The displacements have also been convolved with a 15-100 instrument. Because of the differences in high frequency content between the data and synthetics the displacement responses have been filtered. The filter has an impulse response of a triangle which has a 2 second rise and fall. When comparing these displacements with data, the observations should be similarly filtered. Once the response of the three fundamental faults is known any seismogram can be constructed by a linear combination of them.

The displacements in figure 3 and 4 were computed for a source

depth of 8 km. Varying the source depth between 5 and 15 km has only a small effect on the waveform. This is easily understood by considering that to first order, a change in source depth only affects the travel time of the first segment of any ray. Figure 5 shows a comparison of the synthetics at 1000km for three different source depths. After doubling the source depth (from 8 to 16 km) the essential character of the waveform is still preserved and the source information is retrivable. In contrast, a similar change in crustal thickness would affect the travel time of each leg of a given ray, hence significantly changing the waveform dispersion (Wallace and Helmberger, 1980). The insensitivity of the displacements to source depth allows the responses in figures 3 and 4 to be used, at least in a qualitative fashion, to determine the source parameters of most crustal earthquakes.

The only other major question of applicability of the presented displacements is the structure used in their calculation. Experience indicates that the simplistic model is justified. The model in Table 1 is an average developed for the western U.S. although it appears to be sufficient for most continental regions in the world. The waveform dispersion is dependent on crustal thickness and the contrast between the upper mantle P-velocity and the mean crustal P-velocity, so obviously in regions with anomalous crustal structure such as the Tibetan Plateau the responses in figures 3 and 4 would be inadequate. Also, the use of the halfspace to approximate the upper mantle must break down at some point; at some distance a significant amount of energy will be present in the form of diving rays which have turned in the mantle. For most continental regions this distance appears to be about 12°. If diving rays are present the ratio of the Pn to PL

amplitude should differ from the synthetics (Wallace and Helmberger, 1981). Also, the predicted amplitude should begin to diverge from the observed due to attenuation in the upper mantle. Figure 6 shows a profile of the Truckee records; the amplitudes have been corrected for the azimuthal radiation pattern and the polarit: ~ have been adjusted to show a smooth dispersion pattern. To the right is a profile of displacements for a strike-slip earthquake (such a profile can be constructed from figure 3). Note that there does not appear to a systematic break down in waveform shape or amplitude over the distance range to 4° to 12°. Also note that stations BOZ and TUC are nearly nodal and thus their amplitudes are not particularly reliable.

INVERSION TECHNIQUE

The ability to determine the source parameters of an earthquake by comparing an observed with a predicted waveform depends on the assessment of the quality of fit. In a previous paper (Wallace et al., 1981) we presented a least-squares waveform inversion technique which makes use of an error function determined by the cross-correlation of a long-period seismogram and a synthetic;

$$e = 1 - \frac{\int fg}{\left(\int f^2\right)^{1/2} \left(\int g^2\right)^{1/2}} \tag{3}$$

where f is the observed record, g is the synthetic and the integral is a zero lag cross-correlation. The limits of integration are the time length of the window in which the waveforms are correlated. The denominator serves to normalize both the data and the synthetics. This normalization process makes the error function insensitive to the absolute amplitudes. To minimize the error, which corresponds to

maximizing the correlation, we allow f and g to optimally align themselves with regard to waveform. f and g are aligned a priori in time by matching first breaks and ignoring absolute travel time. The error function can be rewritten by considering that the synthetic seismogram can be constructed with the three fundamental faults. In this case there is a summation of cross-correlations between the observed and each of the fundamental faults. For a given range, the cross-correlations are constant and errors can be minimized by varying the A_i's in equation 2. In other words, once the cross-correlations are computed the source orientation is determined iteratively and only the constants have to be recalculated. For a detailed discussion of the inversion technique see Wallace et al. (1981).

Once the source orientation is fixed, the moment of an earthquake can be determined by comparing the amplitude of the synthetics and observations. Adopting the units of Helmberger and Malone (1975), and expressing the range in km, time in seconds, density in gm/cm^3, velocity in km/sec, the moment in dyne-cm and displacement in cm yields:

$$M_o = 4\pi\rho \times 10^{20} \left(\frac{\text{data amplitude}}{\text{synthetic amplitude}} \right) \qquad (4)$$

A moment can be determined by comparing the maximum peak to peak amplitude for any time window used for the correlation. It has been found that a moment should be determined for a few peaks at a given station. The ratio of the moment at each station to the mean is a measure of the amplitude stability. In general, the moments determined from P_{nl} are in very good agreement with those determined teleseismically, using an assumption of $t^* = 1$ sec.

EXAMPLES

We have inverted the $P_{n\ell}$ waveform from five earthquakes to demonstrate the utility of the technique. Three of the earthquakes are in the western U.S. Two other earthquakes, one in Baffin Bay in the Artic and the other in Turkey, have been included to demonstrate that the Green's functions are not unique to the U.S. Both dip-slip and strike-slip mechanisms are represented in the suite of examples.

Truckee, California (9/12/67)

The Truckee earthquake was a strike-slip event at 10 km depth which produced excellent regional records but very few teleseismic body wave records as typical of moderate size strike-slip events. The Truckee earthquake (m_b=5.7) has been studied by numerous authors (Ryall et al., 1968; Tsai and Aki, 1970; Burdick, 1977) making it a good test case. Tsai and Aki (1970), from first motion studies and modeling of the surface waves, determined this event to be pure strike-slip on a fault plane striking N44°E and dipping 80°SE. The surface wave moment was determined to be 0.83 x 10^{25} dyne-cm. Figure 2 shows the location of the epicenter, recording stations and filtered data for Truckee. Also shown are the synthetics determined from the inversion results. Note that BOZ and TUC are very nearly nodal. The inversion yields a mechanism which is very similar to Tsai and Aki's (1970); a strike of N43°E, a dip of 76°SE and a rake of -11°. The only significant difference is the slight dip-slip component in our solution, which is also acceptable on the basis of the first motion data. The moment determined from the $P_{n\ell}$ waveforms is 0.87 x 10^{25} dyne-cm, which is in

excellent agreement with Tsai and Aki (1970).

El Golfo, Mexico (8/7/66)

The El Golfo earthquake (m_b=6.3, M_s=6.3) is a strike-slip event which occurred near the mouth of the Colorado River at the northern end of the Gulf of California. Ebel et al. (1978) determined the fault plane to be striking E140°S, dipping 85° to the southwest and with a rake of 183°, and determined the depth of the event to be 10 km. Using teleseismic long-period P-waves they determined a moment of 5.0 x 10^{25} dyne-cm.

El Golfo is about the maximum size event which can be used in the inversion technique. The $P_{n\ell}$ records are barely on scale at the stations used. Figure 7 shows the location of the epicenter, recording stations and the waveforms. In this case the time function is a triangle with a two second rise and fall; the long-period impluse is a reflection of the event size. The long-period time function allows us to dispense with using a filter. In figure 7, shown below the observed waveforms are the synthetics for the inversion solution; a strike of E137°S, a dip of 81° and a rake of 175°. The inversion solution is in good agreement with Ebel et al. (1978). The moment determined from the P is 4.6 x 10^{25} dyne-cm.

Oroville, California (8/7/75)

The Oroville earthquake (M=5.6) was a normal faulting event and is interesting because the surface wave (Hart et al., 1977) and body wave (Langston and Butler, 1976) analysis yield substantially different moments. Langston and Butler (1976) determined the strike to be 180°, with a dip of 65° and a rake of -70°. Their moment determination is 5.7 x 10^{24} dyne-cm. Hart et al. (1977) suggests that the surface waves are

consistent with the body wave mechanism but the moment is a factor of 3 larger (1.9×10^{25} dyne-cm). Figure 8 shows the location of the event, the stations used in the inversion analysis and the filtered data and synthetics. The inversion solution has shifted the mechanism to a strike of 204°, dipping 66° and a rake of -85°. This new solution only violates a few first motions, but the aftershock trend tends to support the 180° strike. The moment determined from $P_{n\ell}$ is 6.9×10^{24} dyne-cm.

Baffin Bay, Canada (9/4/63)

The Baffin Bay earthquake (M=5.9) is a normal event associated with a continental margin area. The travel path to each of the stations used in the inversion includes portions of crustal and oceanic regions which makes an ideal event to test the applicability of the Green's functions. Liu and Kanamori (1980) modeled the body waves and determined a fault plane solution with a strike of 98°, dip of 66°N and a rake of -103°. The location of the event and the filtered data and synthetics are shown in Figure 9. The inversion solution has a mechanism striking 74°, dipping 66° and has a rake of -100°. Again the only parameter which is appreciably different from the teleseismic analysis is the strike. In any case the inversion solution is acceptable, and the difference of 20° in strike can be considered the resolution for dip-slip events.

Turkey (6/13/65)

The Turkish event (M=5.1) is a shallow normal event which occurred in southwest Turkey in a region of north-south extension. McKenzie (1972) used first motion data to determine a pure normal mechanism with a strike of 101°, dipping 70° to the south, although it is not well constrained. There were three WWSSN stations at regional distances which could be used in the inversion process. Figure 10 shows the

location of the event and the recording stations. The filtered data and
the fit of the synthetics are also shown. The inversion solution
(strike = 131°, dip = 68°, rake = -88°) is consistent with the first
motion data, although it differs in strike from McKenzie's solution.
Again the three station solution is quite acceptable, considering the
quality of the first motion data.

DISCUSSION

Determining the fault-plane orientation of moderate size
earthquakes is often a frustrating experience due to the paucity of high
quality data. Earthquakes in the magnitude range of 5 to 6 are quite
important and often are the only "measurable" expression of the present
tectonic environment. All the available data must be used to extract
the source parameters of these moderate size events, and the modeling of
$P_{n\ell}$ waveforms can provide a valuable constraint in this process. Every
situation will probably be unique and it is difficult to predict which
data set will be the most definitive. Nevertheless, it appears
worthwhile to consider the $P_{n\ell}$ inversion seperately and its
resolvability dependence on source orientation.

The inverison process we discussed only requires a small data set.
With ideal azimuthal separation, a data set comprised of just 3 stations
(vertical and radial component) can yield good solutions (it is possible
to construct a case where the inversion is unstable, but in practice
this has never happened). In almost all cases 4 recording stations are
sufficient. $P_{n\ell}$ should be polarized in the vertical and radial planes.
Rotation of the horizontal components for a number of events indicates

that there is very little energy on the tangential component implying little contamination from such effects as multipathing. Therefore, it is usually sufficient to take the largest of the horizontal components to be the radial waveform in the inversion. The resolving ability of the inversion (or conversely the error) depends on the type of earthquake. The experience gained by considering the examples presented in the last section indicates that the mechanisms of strike-slip earthquakes can be determined quite well with relatively few stations. The strike is usually determined to within 5° of that determined by other methods. The rake is the least resolvable parameter for strike-slip events and can vary up to 15° from that determined by first motion studies. The mechanisms of dip-slip earthquakes are more difficult to determine. Although the dip and rake are usually determined in good agreement with other studies, the strike may vary up to 20°. This feature is illustrated by considering a 45° dipping normal fault. In this case, most regional stations lie within the compressional region of the focal sphere and any given azimuth will produce remarkably similar waveforms. Fortunately, dip-slip events have rather strong teleseismic P-waves but again the waveforms are all the same with little dependence on azimuth. In this case the stations lie in the center of the focal sphere and are all dilatational. As an example consider Figure 11, which displays the focal sphere and the teleseismic waveforms for the Oroville earthquake. Note that the P-waveforms are all similar and the synthetics (Langston and Butler, 1976) do not add much insight into determining the strike of the fault. Figure 12 shows the filtered regional data and synthetics computed from the teleseismic fault parameter determinations. A comparison of figure

12 and 8 will show that the regional data inversion solution improves
the fit of the synthetics, in particular PAS. This suggests that a
logical approach would be to invert some teleseismic data and the
regional data simultaneously. Since the inversion technique relies on
the cross-correlation of data and a synthetic the joint inversion is
quite tractable.

The higher resolution of the strike-slip events is actually
fortuitous. Moderate size strike-slip earthquakes rarely produce usable
teleseismic P-waves due to their inefficiency in radiating energy
straight down. On the other hand, strike-slip events produce very good
regional waveforms. This allows the inclusion of a larger data set in
the inversion and hence, the resolution problem is at least partially
resolved.

It is reasonable to consider what effect the structual model has on
the inversion results. As a test of the insensitivity of the fault
orientation to small changes in crustal parameters the El Golfo
earthquake was reinverted with a different structure. The crustal
thickness was reduced to 24 km, the source depth was moved to 12 km and
the Pn velocity reduced to 7.8 km/sec. Although the quality of the fit
decreases significantly the mechanism returned by the inversion is
similar; strike is 138°, dip is 82° and a rake of 181°. The moment
increases to 6.9×10^{25} dyne-cm.

CONCLUSIONS

It is possible to extract the source parameters of moderate size
earthquakes from the long-period regional body waves. The procedure
requires the comparison of the observed waveform with a synthetic; the

synthetics can be generated by a linear combination of the waveforms of the three fundamental faults shown in figures 3 and 4. Although these synthetics are for a single model the inversion parameters (fault strike, dip and rake) are fairly insensitive to small changes in crustal thickness, Pn velocity and mean crustal velocity. This allows this single set of Green's functions to be used for most continental earthquakes. The inversion procedure only requires a small data set, and is particularly ideal for strike-slip earthquakes.

ACKNOWLEDGEMENTS

REFERENCES

Burdick, L.J., Broad-band seismic studies of body waves, Ph.D. thesis, Calif. Inst. of Technol., Pasadena, 1977.

Ebel, J.E., L.J. Burdick and G.S. Stewart, The source mechanism of the August 7, 1966 El Golfo earthquake, Bull. Seismol. Soc. Am.,68, 1281-1292, 1978.

Hart, R.S., R. Butler, and H. Kanamori, Surface-wave constraints on the August 1, 1975 Oroville earthquakes, Bull. Seismol. Soc. Am., 68, 301-316, 1977.

Helmberger, D.V., Generalized ray theory for shear dislocations, Bull. Seismol. Soc. Am., 64, 45-64, 1974.

Helmberger, D.V., and G.R. Engen, Modeling the long-period body waves from shallow earthquakes at regional distances, Bull. Seismol. Soc. Am., 70, 1699-1714, 1980.

Helmberger, D.V., and S.D. Malone, Modeling local earthquakes as dislocations in a layered half space, J. Geophys. Res., 80, 4881-4888, 1975.

Langston, C.A. and R. Butler, Focal mechanism of the August 1, Oroville earthquake, Bull. Seismol. Soc. Am., 66, 1111-1120, 1976.

Langston, C.A. and D.V. Helmberger, A procedure for modeling shallow dislocations, Geophy. J. R. Astron. Soc., 42, 117-130, 1975.

Liu, H.L. and H. Kanamori, Determination of source parameters of midplate earthquakes from the waveforms of bodywaves, Bull. Seismol. Soc. Am., 70, 1989-2004, 1980.

McKenzie, D., Active tectonic of the Mediterranean region, Geophys. J. R. astr. Soc., 30, 109-185, 1972.

Ryall, A., J.D. Van Wormer, and A.J. Jones, Triggering of microearthquakes by earthtides and other features of the Truckee, California earthquake sequence of September, 1966, Bull. Seismol. Soc. Am., 66, 215-248, 1968.

Tsai, Y.B., and K. Aki, Source mechanism of the Truckee, California earthquake of September, 12, 1966, Bull. Seismol. Soc. Am., 60, 1199-1208, 1970.

Wallace, T.C. and D.V. Helmberger, Some useful approximations for modeling $P_{n\ell}$, EOS, 61, p1046, 1980.

Wallace, T.C. and D.V. Helmberger, A procedure to account for the effects of upper mantle gradients on $P_{n\ell}$, Earthquake Notes, 52, p32,

1981.

Wallace, T.C., D.V. Helmbeger and G.R. Mellman, A technique for the inversion of regional data in source parameter studies, J. Geophy. Res., 86, 1679-1685, 1981.

TABLE 1 - CRUSTAL MODEL

P_{vel}(km/s)	S_{vel}(km/s)	Density (gm/cc)	Layer Thickness (km)
6.2	3.5	2.7	32
8.2	4.5	3.4	

Figure 1: The horizontal component of motion for four moderate size earthquakes. The magnitude and distance to the recording station is given for each. Clockwise from the upper left; (1) Sept. 12, 1966, Truckee, California, a strike-slip event, (2) June 13, 1965, southwest Turkey, a normal event, (3) Aug. 7, 1975, Oroville, California, a normal event, and (4) Dec. 10, 1967, off the coast near Cape Mendocino, California, a strike-slip event.

Figure 2: The vertical $P_{n\ell}$ waveforms of the 1966 Truckee earthquake. The star denotes the epicenter. The data is the top trace at each station and the trace below is the synthetic fit. The strike-slip mechanism has two nodal planes which project through TUC and BOZ. To the right of each trace is the observed or predicted amplitude (on the basis of .8 x 10^{25} dyne-cm) in 10^{-3} cm.

Figure 3: Theoretical displacement profiles for the vertical component. The Green's fuctions were computed from the model presented in Table 1 and have been convolved with a source time function represented by a trapezoid (t_1=1,t_2=1,t_3=1), a triangular filter (2 second rise and fall), and a WWSSN long-period instrument.

Figure 4: Displacement profiles for the radial component. The Green's functions are computed every 100 km. They have been convolved with the time function, instrument and filter discribed in figure 3.

Figure 5: $P_{n\ell}$ waveforms at 1000 km for three different source depths.

Figure 6: The Truckee waveforms have been corrected for horizontal radiation pattern and plotted as a function of distance. The maximum amplitude is shown to the right of each trace. Note that BOZ and TUC are very close to nodes.

Figure 7: Data and synthetics from the El Golfo earthquake. The map gives the location of the event (star) and the recording stations. Along each trace is the ratio of the station moment and the average moment.

Figure 8: Filtered data and synthetics from the Oroville earthquake. At all the stations except GOL both the vertical (the first trace pair) and radial components are shown.

Figure 9: Location of the Baffin Bay earthquake (star) and the recording stations. The filtered data and synthetics from both the vertical and radial components are shown.

Figure 10: Location of the Turkey event (star) and the recording stations. The filtered data and synthetics for both the vertical and radial components are shown.

Figure 11: The teleseismic waveforms from the Oroville earthquake. Note the similarity of the wavefoms at all azimuths. Shown on each trace is the moment (x 10^{25} dyne-cm) determined at that station. Note

the factor of 3 scatter (figure from Langston and Butler, 1976).

Figure 12:   Filtered $P_{n\ell}$ from the Oroville earthquake.   The synthetics were computed with the teleseismic fault plane solution.
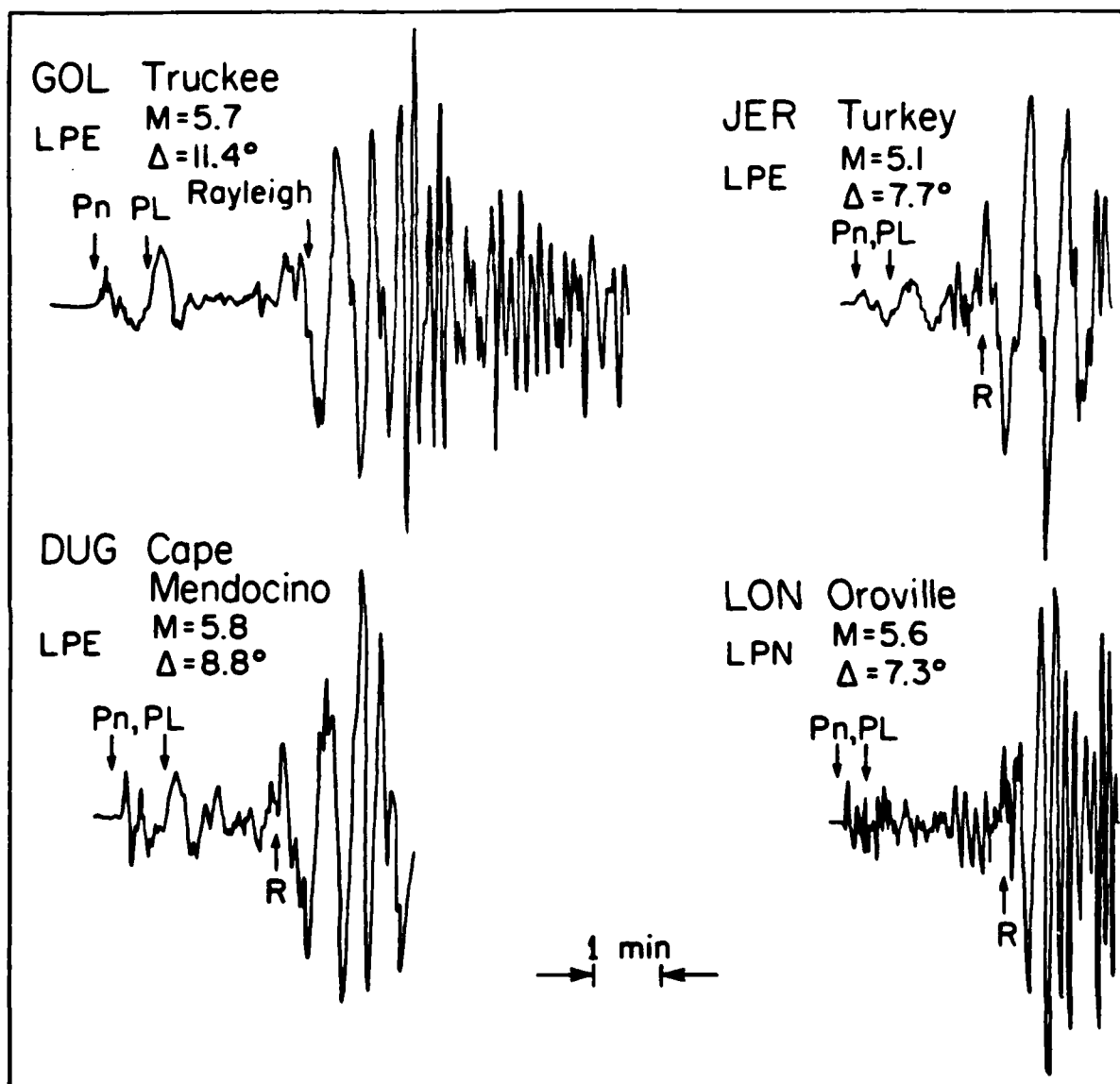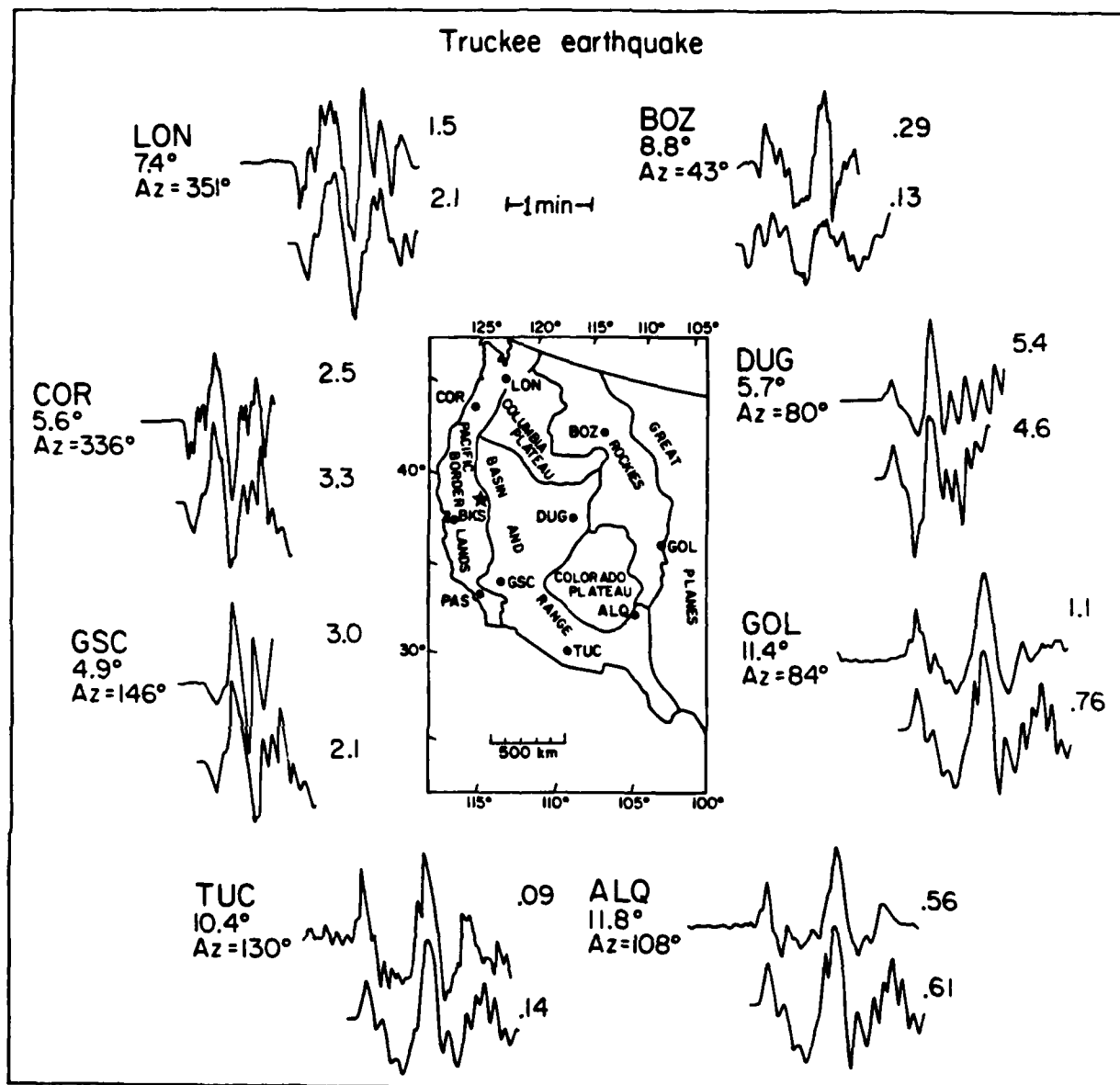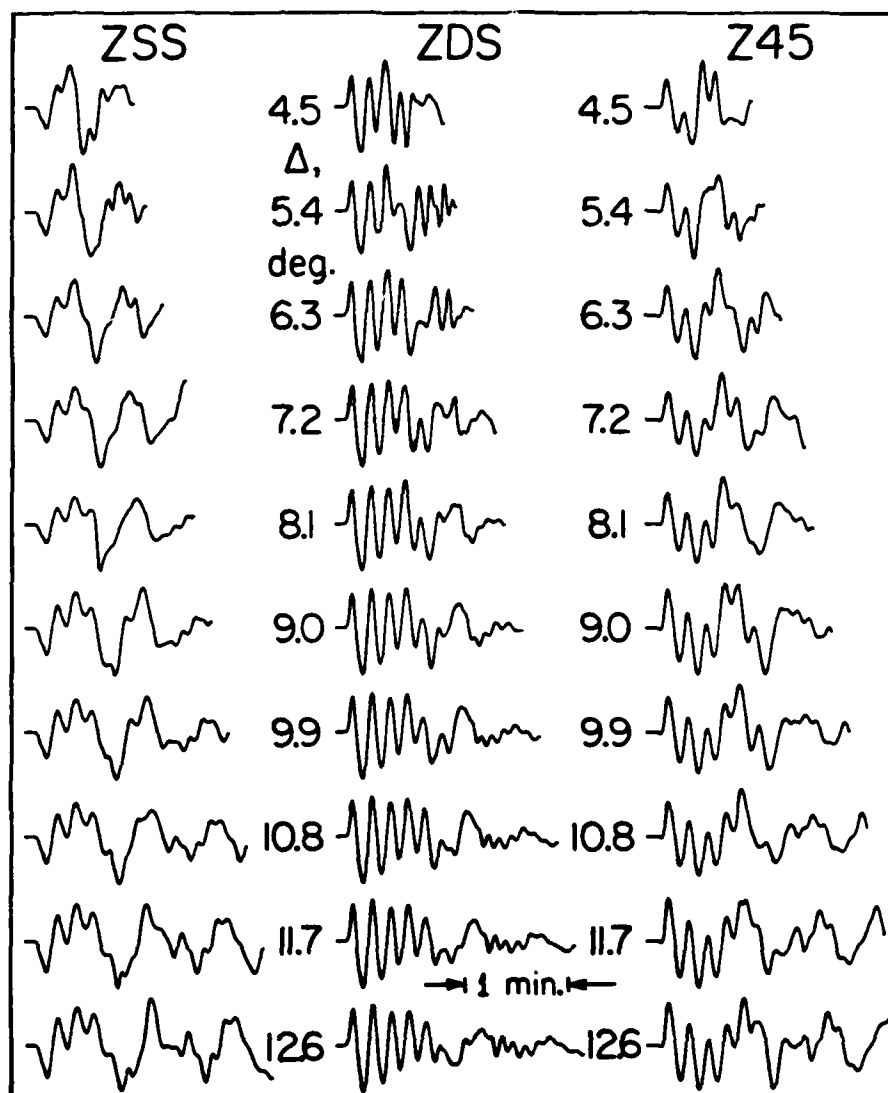
Fig. 1

Truckee earthquake
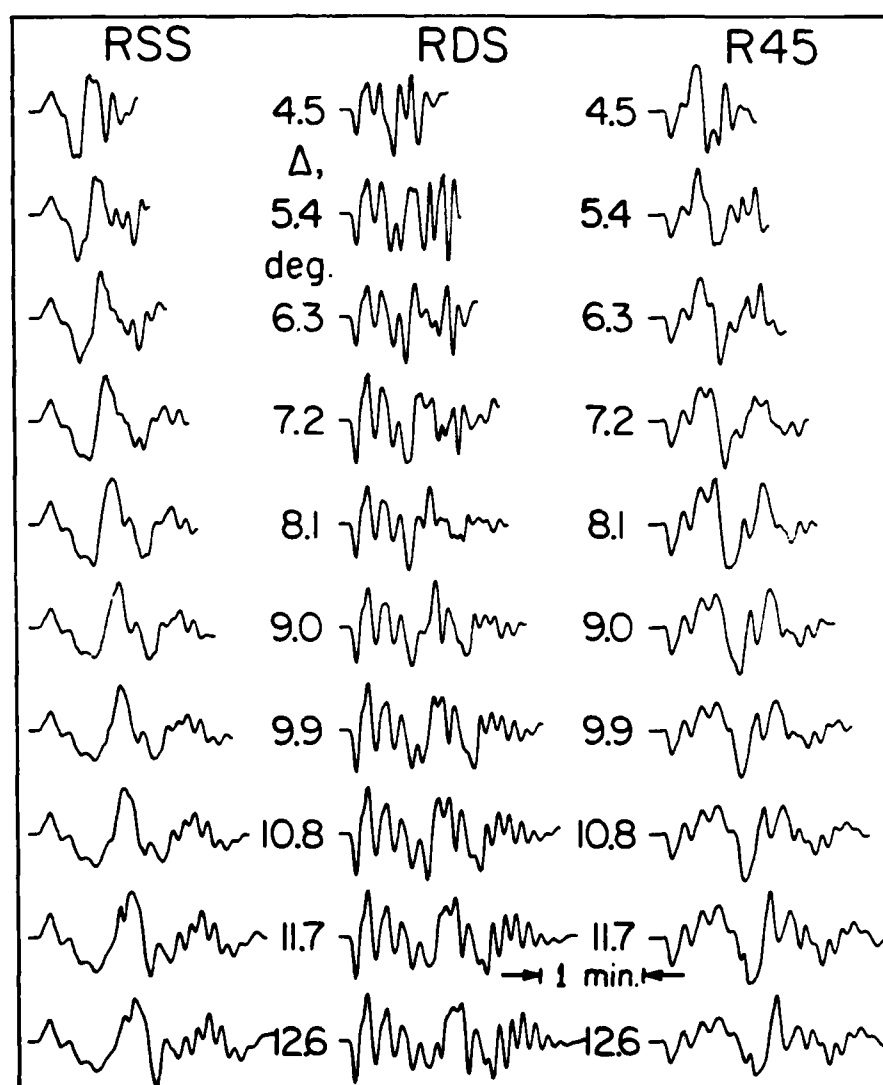
Fig. 2

48

Fig. 3

Fig. 4

Fig. 5

Dilatational

Fig. 6

Pocatello 3/28/75

Fig. 7

OROVILLE (INVERSION)
$\theta = 204°$
$\delta = 66°$
$\lambda = 275°$

Fig. 8

BAFFIN BAY 9/4/63
$\theta = 74°$
$\delta = 66°$
$\lambda = 260°$

ALE
$\Delta = 11.5°$
$Az = 7°$

RES
$\Delta = 7.2°$
$Az = 308°$

Vert.

Rad.

GDH
$\Delta = 7.0°$
$Az = 97°$

⊢1 min⊣

Fig. 9

TURKEY 6/13/65

$\theta = 131°$

$\delta = 68°$

$\lambda = 272°$

Fig. 10

Fig. 11

OROVILLE
$\theta = 180°$
$\delta = 65°$
$\lambda = -70°$

LON
$\Delta = 7.3°$
$Az = 358°$

MSO
$\Delta = 9.2°$
$Az = 34°$

COR
$\Delta = 5.3°$
$Az = 346°$

GOL
$\Delta = 12.5°$
$Az = 83°$

TUC
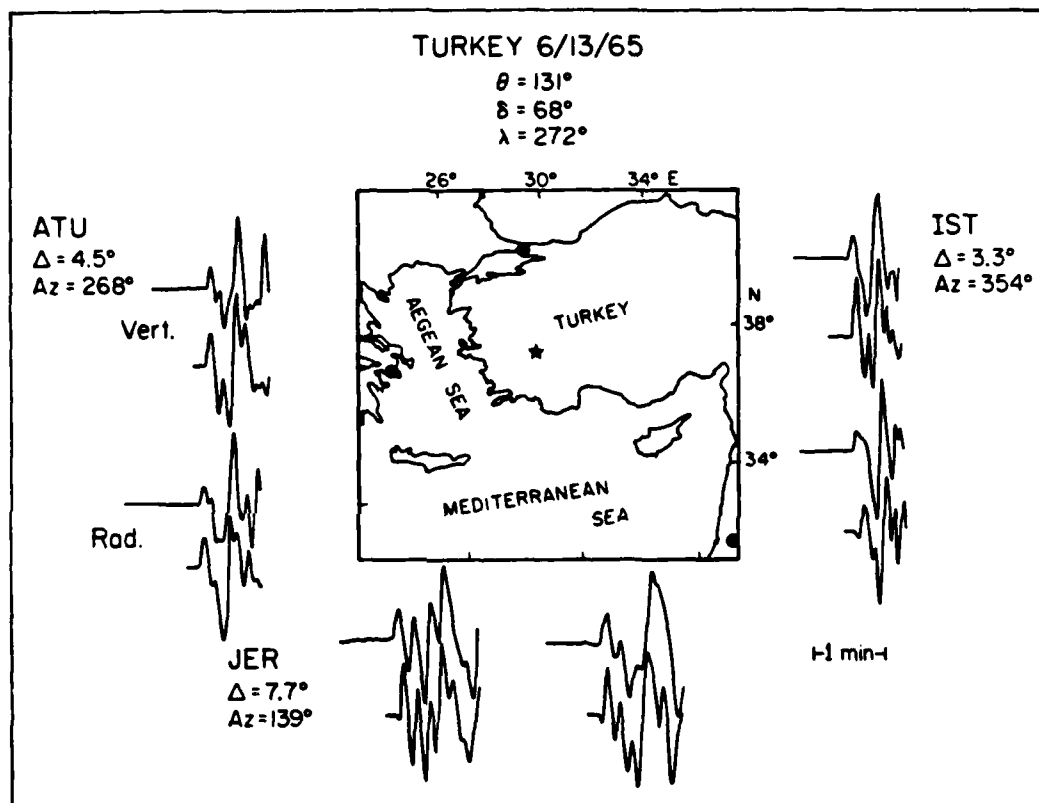$\Delta = 11.2°$
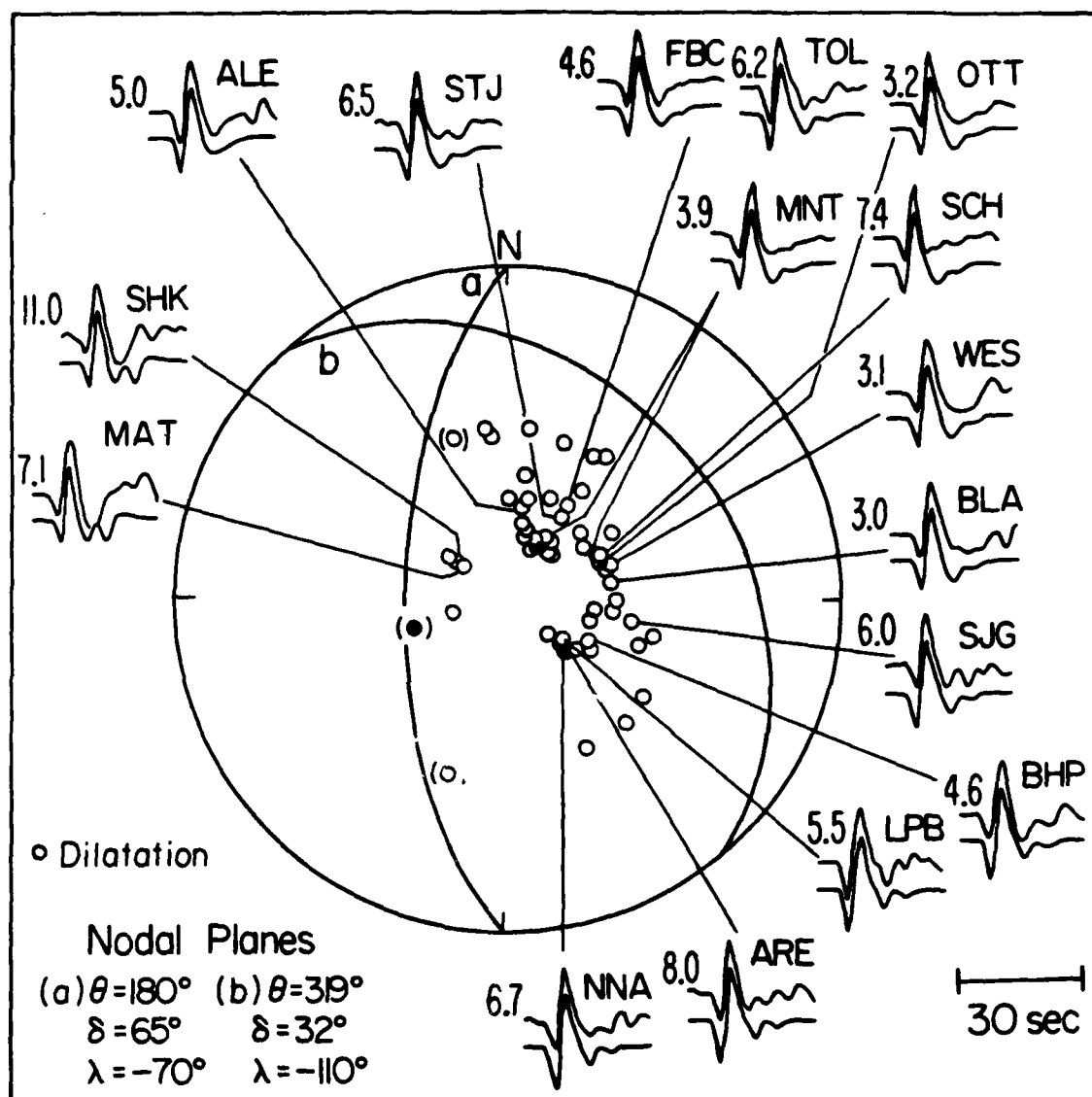$Az = 125°$

PAS
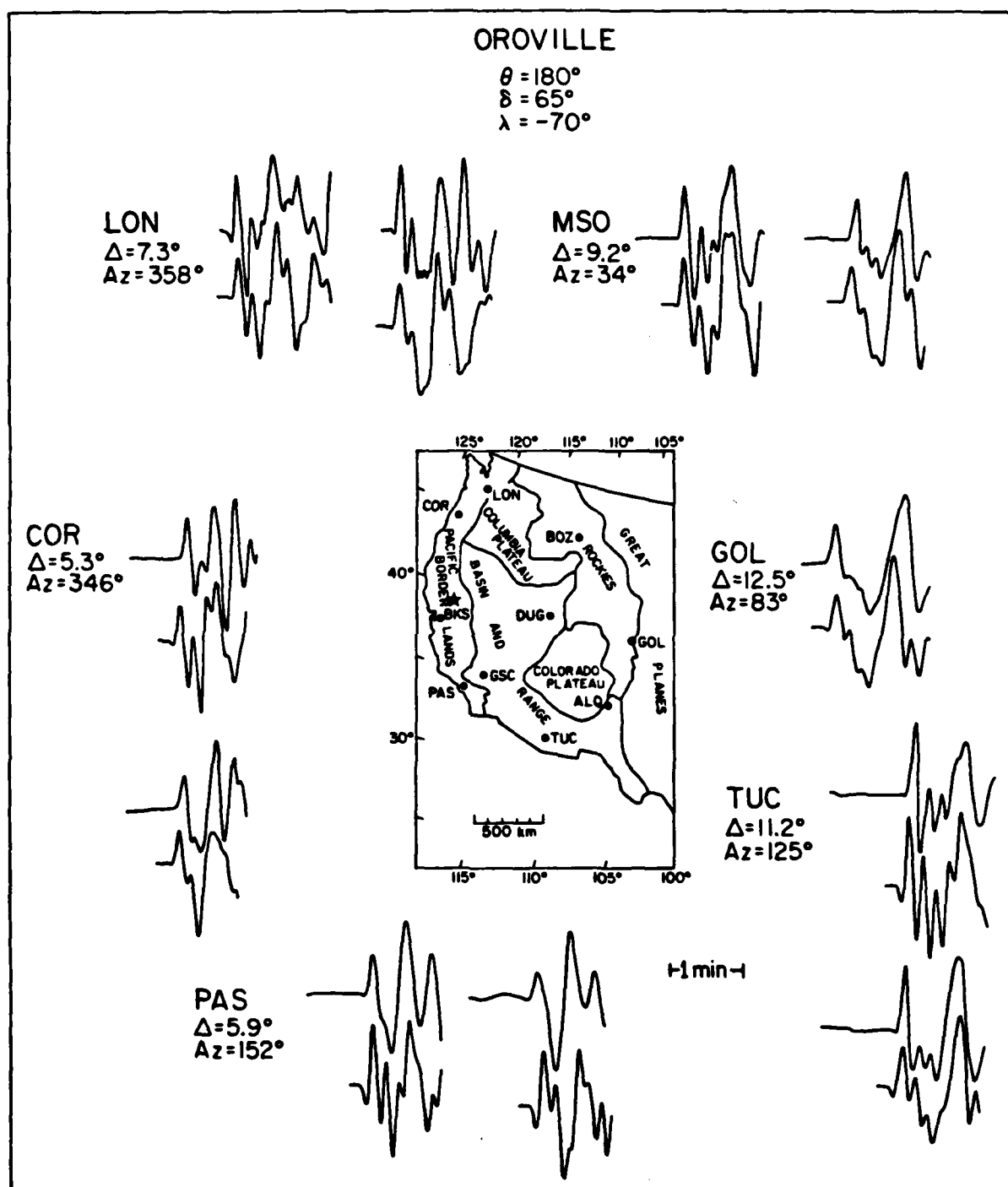$\Delta = 5.9°$
$Az = 152°$

⊢1 min⊣
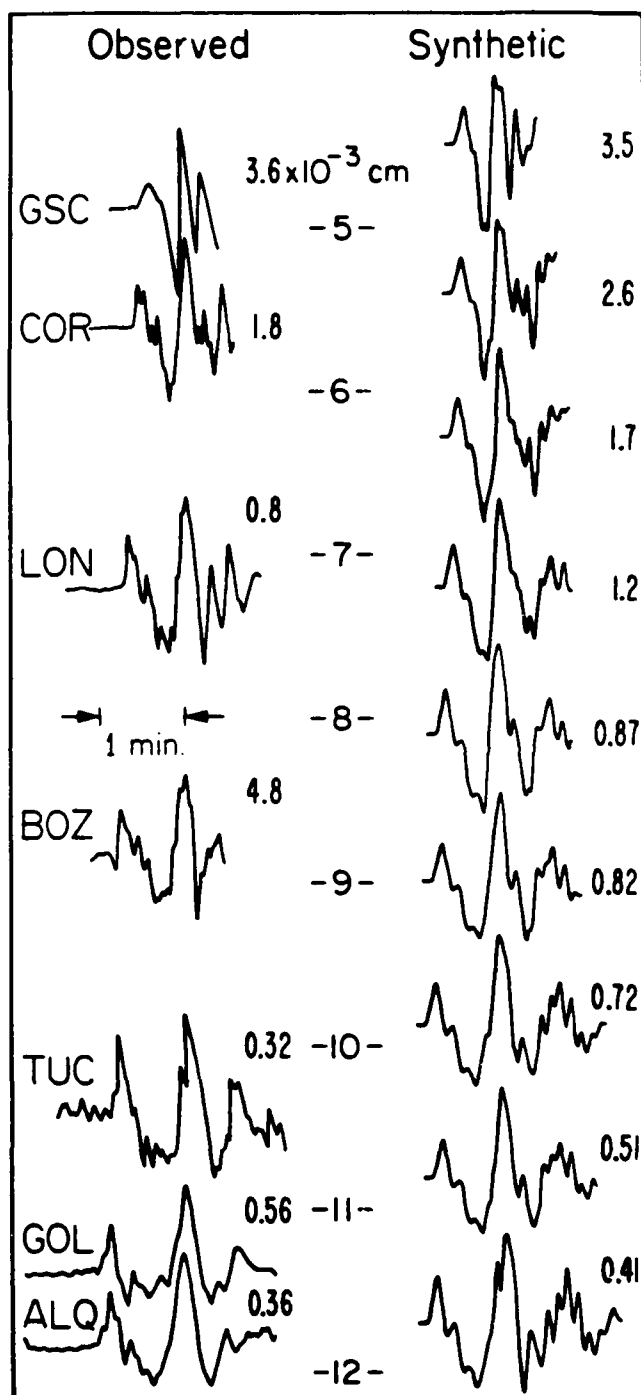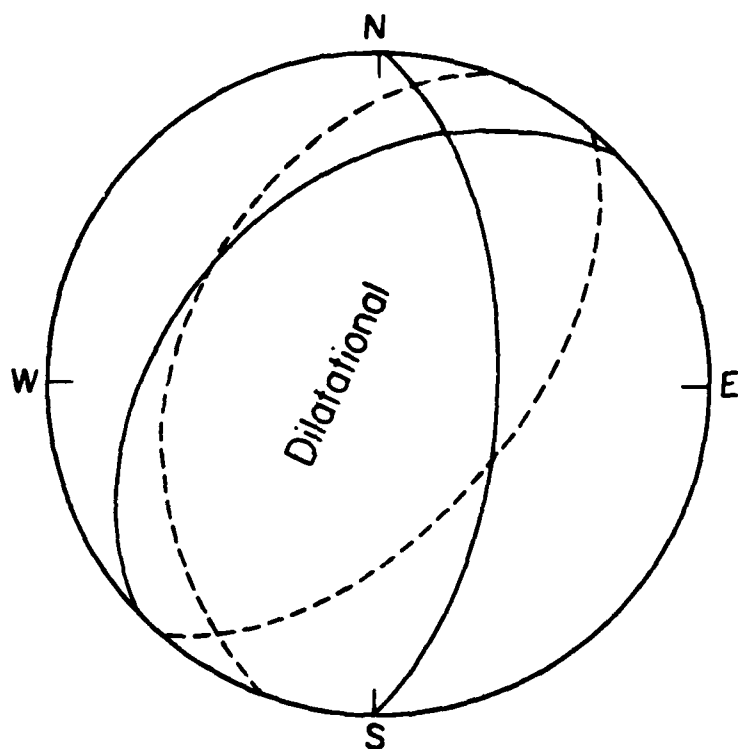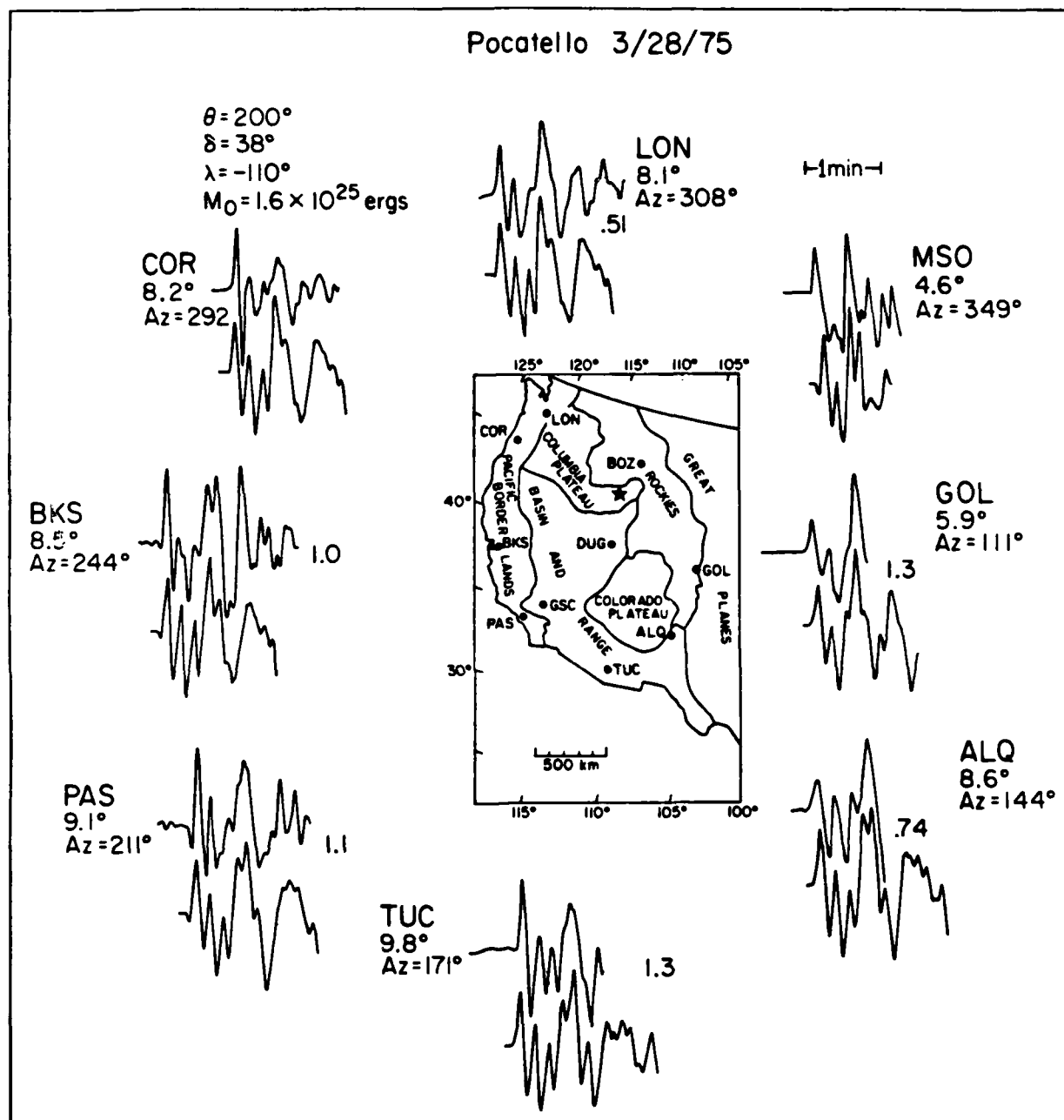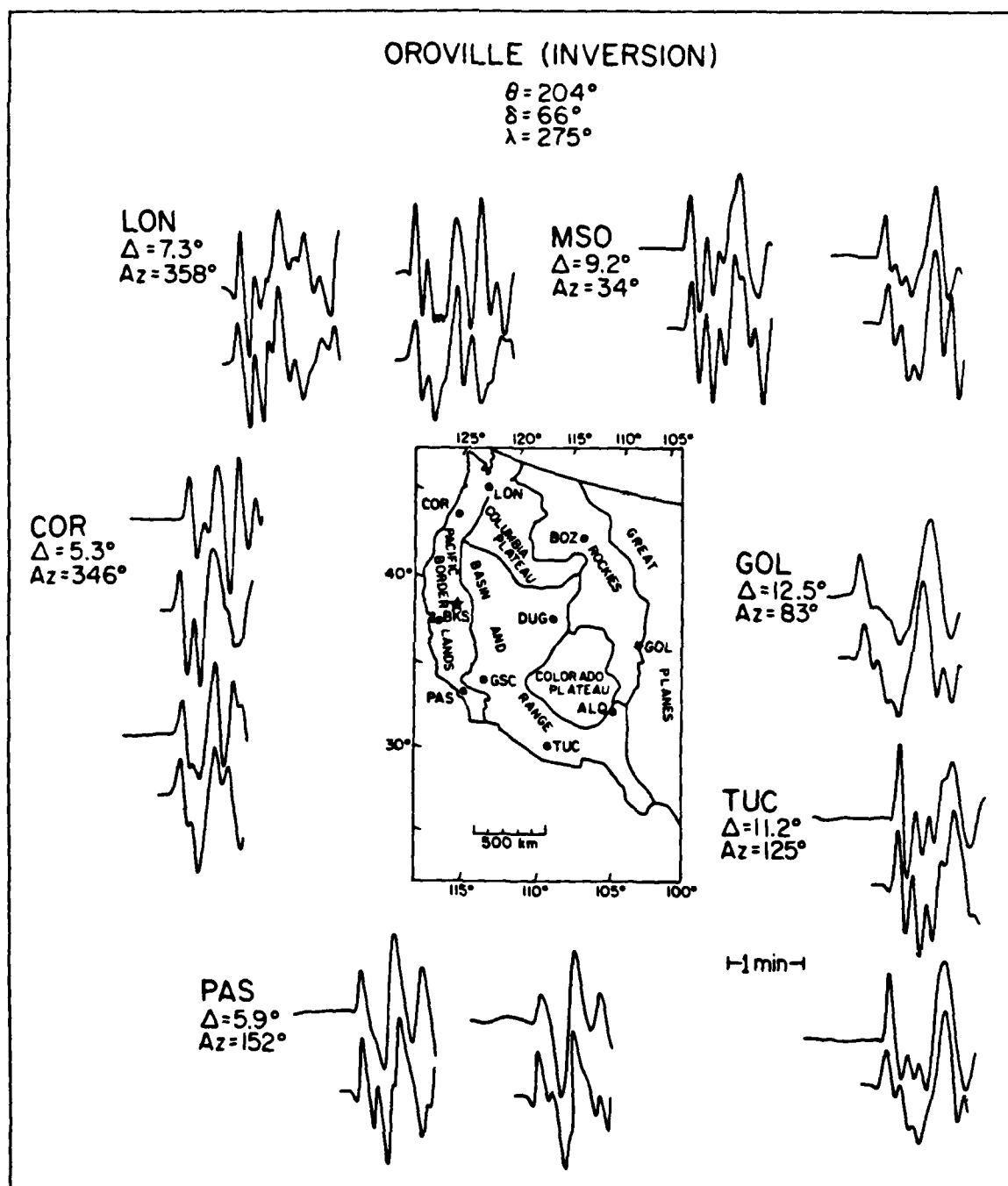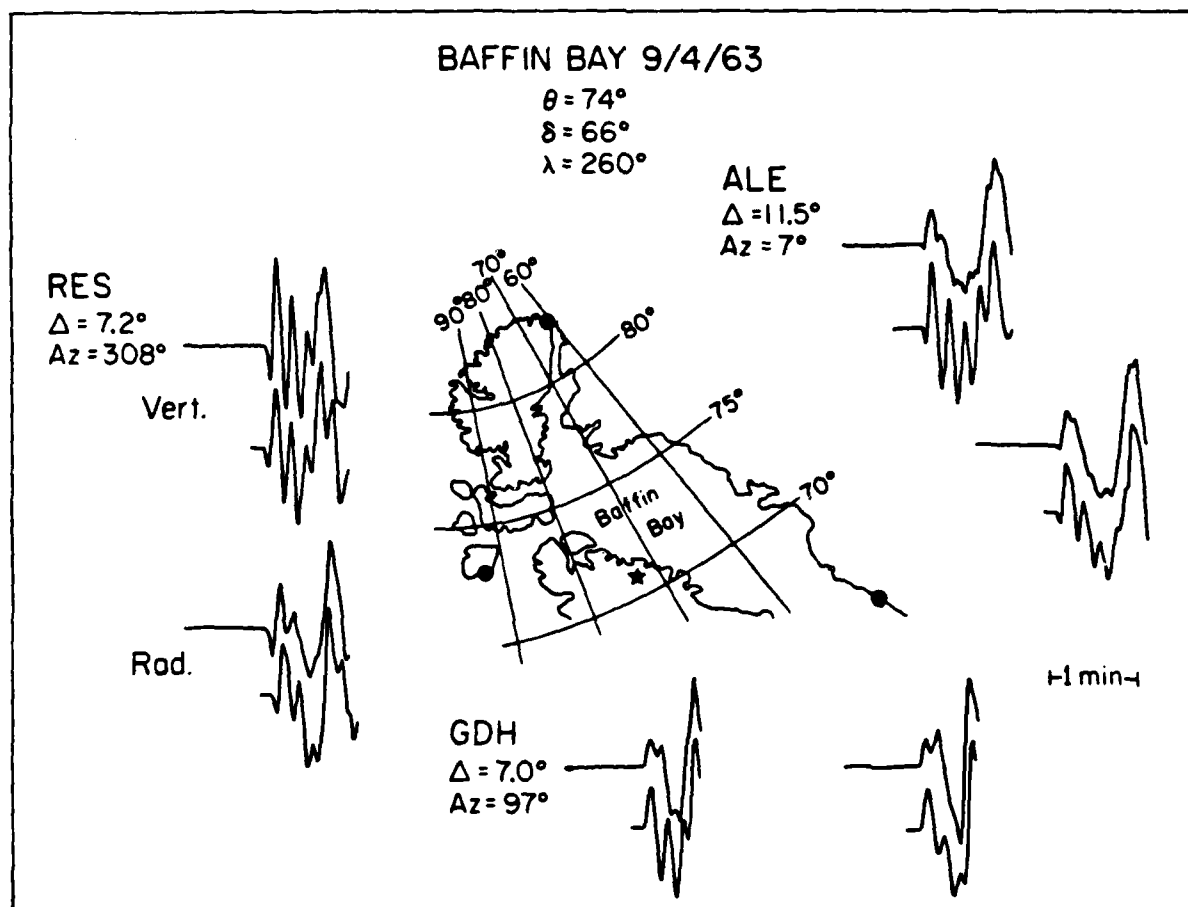
Fig. 12

APPLICATIONS OF THE KIRCHHOFF-HELMHOLTZ INTEGRAL TO
PROBLEMS IN SEISMOLOGY

PATRICIA SCOTT

AND

DON HELMBERGER

Seismological Laboratory,

California Institute of Technology,

Pasadena,

California 91125, USA

ABSTRACT

A numerical method for evaluating the Kirchhoff-Helmholtz integral is described. The Kirchhoff response is calculated by discretizing the surface, specifying simple point sources on each element of the surface, and summing the contribution from the elements. The results of the method are compared to those of an asymptotic, first motion approximation of the analytical solution of SH waves impinging on a rigid sphere. The agreement between the results of the two methods is excellent for source and receiver distances which are large compared to the radius of the sphere. The method is applied to the calculations of reflections from mountain topography and a planar surface with an aperture. The phase shifts of pulses are consistent with optics; the amplitudes are not. The method does predict frequency dependence of the scattered amplitudes. Calculations are presented to model spall which produce travel-time and amplitude anomalies consistent with observations from nuclear blasts.

Introduction

Many wave propagation phenomena cannot be adequately modeled by existing solutions to plane-layered media. Yet the increasing use of broad-band seismic data to determine source dislocations, Q, and velocity structure requires a knowledge of effects of material irregularities in the medium on seismic wave propagation. Certainly, documented amplitude and $dT/d\Delta$ anomalies of teleseismic arrivals at large arrays (Glover and Alexander, 1969; Walck and Minster, 1980) which vary as a function of azimuth suggest the existence of non-flat boundaries at depth.

Numerical schemes which handle material irregularities are in abundance. Finite difference and finite element codes have been used successfully (Boore, 1971; Smith, 1975) and can be applied to a variety of materials; however, the expense of calculating the response at distances which are large compared to the wavelength of interest is prohibitive. Rayleigh-FFT techniques have been exploited for these problems (Aki and Larner, 1970). Similiarly, implementation of these methods for analysis of three dimensional scattering is also costly. Geometric ray methods are useful for predicting scattering of signals which have wavelengths that are short compared to the size of the heterogeneity (Hong and Helmberger, 1978). But, existing ray methods do not predict frequency-dependent amplitudes of scattered pulses and do not handle diffracted arrivals.

Discussion of techniques

The method presented in this paper is an integral equation approach
and is based on the evaluation of the scalar integral equation variously
called the Kirchhoff, Helmholtz, or Huygen's integral. This equation is
a formulation of the wave equation in terms of a linear surface integral
over the boundary of a continuous volume. That is, the scalar wave
equation is

$$\frac{1}{c^2}\frac{\partial^2 u}{\partial t^2}(\underline{r},t) - \nabla^2 u(\underline{r},t) = \phi(r_0,t) \tag{1}$$

Here $u(\underline{r},t)$ is the field at a point r resulting from a source potential
$\phi(\underline{r}_0,\underline{t})$ and c is the wave speed. Following the formalism discussed by
Mow and Pao (1971), we consider the motion of a homogeneous body V with
a smooth boundary ∂V with outward pointing normal $\underline{n}$. Then if $\underline{r} \in V$ and
$t \in (0,\infty)$

$$\begin{aligned}
u(\underline{r},t) &= \oint_V \int_0^\infty G(\underline{r},\underline{r}_0,t-t_0)\phi(\underline{r}_0,t)dt_0 dV_0 \\
&+ \int_V \left\{ G(\underline{r},\underline{r}_0,t)\frac{\partial u}{\partial t}(\underline{r}_0,0) - u(\underline{r}_0,0)\frac{\partial G(\underline{r},\underline{r}_0,t)}{\partial t} \right\} dV \\
&+ \int_{\partial V}\int_0^\infty \left\{ G(\underline{r},\underline{r}_0,t-t_0)\underline{\nabla}_0 u(\underline{r}_0,t) - u(\underline{r}_0,t)\underline{\nabla}_0 G(\underline{r},\underline{r}_0,t-t_0) \right\} \cdot \\
&\quad \underline{n}(\underline{r}_0)dt_0 dS_0
\end{aligned} \tag{2}$$

Here $G(\underline{r},\underline{r}_0,t-t_0)$ is the fundamental singular solution of the scalar
wave equation

$$\frac{1}{c^2}\frac{\partial^2 G}{\partial t^2} - \nabla_0^2 G(\underline{r},\underline{r}_0,t-t_0) = \delta(t-t_0)\delta(\underline{r}-r_0) \tag{3}$$

Let us define $f(\underline{r},t)$ as the sum of the first two integrals in equation (2). Then $f(\underline{r},t)$ can be interpreted as the whole-space solution of the problem with sources $\Phi(\underline{r}_0,t_0)$ and initial values $\frac{\partial u}{\partial t}(\underline{r}_0,0)$ and $u(\underline{r}_0,0)$. Hence $u(\underline{r},t)$ is a sum of the direct pulse and a reflected pulse from the surface which is described by the third integral in equation (2).

If $\underline{r} \notin V$, then the left-hand side of equation (2) is zero. If $\underline{r} \in \partial V$ then

$$\frac{1}{2}u(\underline{r},t) = \int_0^\infty P\!\!\int_{\partial V} \left\{ G(\underline{r},\underline{r}_0,t-t_0)\underline{\nabla}_0 u(\underline{r}_0,t) - u(\underline{r}_0,t)\underline{\nabla}_0 G(\underline{r},\underline{r}_0,t-t_0) \right\}$$

$$\cdot \underline{n}(\underline{r}_0)\, dt_0\, dS_0 + f(\underline{r},t) \tag{4}$$

Here P denotes the principal value of the integral. A detailed derivation of equation (4) can be found in Cole (1980). This result requires that G has a specific asymptotic behavior at its singularity. The function G used in the Kirchhoff formulation here meets this requirement; Specifically

$$G(\underline{r},\underline{r}_0,t-t_0) = \frac{\delta(t-\tau)}{4\pi\ |\underline{r}-\underline{r}_0|}\ ;\ \tau = \frac{|\underline{r}-\underline{r}_0|}{c} \tag{5}$$

Substitution of this function into equation (2) gives a familiar optics formula (Born and Wolf, 1964)

$$u(\underline{r},t) = \int \frac{1}{4\pi} \left\{ \frac{1}{r} \left[\frac{\partial u}{\partial n}\right] - \left[u\right] \frac{\partial r}{\partial n} \frac{\partial}{\partial r}\left(\frac{1}{r}\right) + \frac{1}{rc} \frac{\partial r}{\partial n} \left[\frac{\partial u}{\partial t}\right] \right\} dS_0 \tag{6}$$

$$+ f(\underline{r},t)$$

where $\underline{r} = |\underline{r}-\underline{r}_0|$, the distance from receiver to surface, $\frac{\partial u}{\partial n} = \underline{\nabla u} \cdot \underline{n}$ and $\frac{\partial r}{\partial n} = \nabla |\underline{r}-\underline{r}_0| \cdot \underline{n}$. The square brackets denote the values of the functions on ∂V at the time $t - |\underline{r}-\underline{r}_0|/c$.

The integrals (2), (4), and (6) are formally exact and are a mathematical representation of Huygen's principle; that is, a disturbance at a receiver point is a superposition of secondary waves proceeding from a surface existing between that point and the source. Diffraction phenomena arise from the mutual interference of these secondary disturbances. However, one needs the value of the potential and its normal derivative on the surface to calculate $u(\underline{r},t)$. Equation (4) may be solved for $u(\underline{r},t)$ or $\underline{\nabla u} \cdot \underline{n}$ on the surface subject to some constraints imposed by boundary conditions (e.g. continuity of $u(\underline{r},t)$ or $\nabla u \cdot \underline{n}$ across the boundary). This approach is taken by Mitzner (1967) who sets $\nabla u \cdot \underline{n}$ equal to zero and solves for $u(\underline{r},t)$. However this approach may be costly for high frequency scattering.

Alternatively one may estimate the values on the surface by invoking an approximation. This approach is used in this paper. Assuming a point source, the boundary values on the surface are taken to be

$$u(\underline{r},t) = \left(f\left(t - \frac{r_0}{c}\right) \middle/ r_0 \right)\left(1 + R\right) \tag{7}$$

$$\frac{\partial u}{\partial n} = \frac{\partial r_0}{\partial n}\left(1 - R\right)\left(-f\left(t - \frac{r_0}{c}\right)\middle/ r_0^2 - \frac{1}{c} f'\frac{\left(t - \frac{r_0}{c}\right)}{r_0}\right) \tag{8}$$

Here r_0 is the distance from the source to the surface, R is the

approximate plane-wave flat interface reflection coefficient, and f(t) and f'(t) are the source time function and its derivative, respectively. The reflection coefficient will depend on incidence angle. This approximation is variously called the Kirchhoff, physical optics, or the tangent plane hypothesis and is widely used by workers in electromagnetic scattering investigations (Davies,1954). It assumes that the incident pulse is sufficiently high frequency so that locally the amplitude decay is described by both geometric ray theory and plane-wave reflection coefficients. Therefore every point on the surface reflects the incident pulse as though there were an infinite plane tangent to the surface at that point. The values of the potential and its normal derivative at a point is independent of the boundary values at other points. Hence the effects of multiple scattering and diffractions along the surface are neglected.

Upon substituting the values (7) and (8) for u and $\frac{\partial u}{\partial n}$ one obtains for the reflected potential

$$u_r(\underline{r},t) = \frac{1}{4\pi} \int_{\partial V} R \left\{ \frac{1}{rr_o^2} \frac{\partial r_o}{\partial n} + \frac{1}{rr_o^2} \frac{\partial r}{\partial n} \right\} f\left(t - \frac{r}{c} - \frac{r_o}{c}\right) dS_o$$

$$+ \frac{1}{4\pi} \int_{\partial V} R \left\{ \frac{1}{crr_o} \frac{\partial r_o}{\partial n} + \frac{1}{rr_o c} \frac{\partial r}{\partial n} \right\} f'\left(t - \frac{r}{c} - \frac{r_o}{c}\right) dS_o \qquad (9)$$

This equation is similar to those derived by A.W.Trorey (1970, 1977), F.J. Hilterman (1970, 1975), and Berryhill (1977). These authors have derived convolutional forms of the Kirchhoff integral which make computation rapid. Hilterman has verified his results with small scale experimental modeling of a point source in air impinging on rigid

anticlines, synclines, and normal faults. The agreement between his numerical calculations and experiments is, in general, excellent. However, these analytical forms of the solution place severe restrictions on either the source-receiver geometry or the surface geometry.

The method presented in this paper differs from Trorey and Hilterman in that the source and receiver are allowed to be at separate locations, the surface geometry is arbitrary, and the integral is approximated by the following expression

$$u_r(\underline{r},t) = \frac{1}{4\pi} \sum_{k=1}^{N} R \left\{ f\left(t - \frac{r_o}{c} - \frac{r}{c}\right) Q_k^{(1)} + f'\left(t - \frac{r_o}{c} - \frac{r}{c}\right) Q_k^{(2)} \right\} \Delta S_k \qquad (10)$$

where

$$Q_k^{(1)} = \frac{1}{rr_o^2} \frac{\partial r_o}{\partial n} + \frac{1}{r_o r^2} \frac{\partial r}{\partial n}$$

and

$$Q_k^{(2)} = \frac{1}{rr_o c} \frac{\partial r_o}{\partial n} + \frac{1}{rr_o c} \frac{\partial r}{\partial n}$$

An important part of the procedure is the discretization of the surface. The rough surface is specified by a function $z(x_i, y_i)$ where (x_i, y_i) is a location on a horizontal grid of regularly spaced points separated by a distance Δx and Δy (see Fig. 1). From this information, one can readily calculate $\frac{\partial z}{\partial x}$ and $\frac{\partial z}{\partial y}$. Then the following formulae are used to calculate ΔS_k, $\frac{\partial r_o}{\partial n}$, and $\frac{\partial r}{\partial n}$:

$$\Delta S = \sqrt{1 + \left(\frac{\partial z}{\partial x}\right)^2 + \left(\frac{\partial z}{\partial y}\right)^2} \; \Delta x \Delta y \qquad (11)$$

$$\frac{\partial r}{\partial n} = \frac{\left((x_s-x_1)\frac{\partial z}{\partial x} + (y_s-y_1)\frac{\partial z}{\partial y} - (z_s-z_1) \right)}{r \quad \sqrt{1 + \left(\frac{\partial z}{\partial x}\right)^2 + \left(\frac{\partial z}{\partial y}\right)^2}} \tag{12}$$

$$\frac{\partial r_o}{\partial n} = \frac{\left((x_o-x_1)\frac{\partial z}{\partial x} + (y_o-y_1)\frac{\partial z}{\partial y} - (z_o-z_1) \right)}{r_o \quad \sqrt{1 + \left(\frac{\partial z}{\partial x}\right)^2 + \left(\frac{\partial z}{\partial y}\right)^2}} \tag{13}$$

Here x_s, y_s, and z_s are the station coordinates and x_o, y_o, and z_o are the source coordinates. These values are calculated for a finite surface. However the Kirchhoff integral is formally stated for a closed surface. This problem is circumvented by integrating over a closed surface consisting of the part of the surface one is interested in (S) and a portion of a sphere of large radius (S_β) (see Fig. 2). One then argues that the contributions from the sphere arrive at the receiver at times later than those of interest and neglects them.

For the time function $f(t)$ we have chosen a ramp function. This choice circumvents the problems of numerically simulating a delta function. So, on each element we add the sum of a ramp function multiplied by $Q_k^{(1)}$ and a step function multiplied by $Q_k^{(2)}$ appropriately in time. That is, each element is illuminated and contributes to the total response at a time $\tau = (r+r_o)/c$. This two-way travel time is calculated and the responses from all the elements are summed cumulatively in order of increasing τ as displayed in Fig. 3.

For problems presented in this paper, the numerical ramp response is convolved with the analytical third derivative of a modified Haskell explosion source function, specifically

$$\Psi(t) = \Psi_o \left[1 - e^{-kt}\left(1 + kt + (kt)^2/2 - B(kt)^3 \right) \right] \tag{14}$$

Here Ψ_0 is the source strength, k scales inversely as the source strength and B is the overshoot constant. This convolution is mathematically equivalent to the first derivative of the reflected potential caused by a source described by (14). From trial and error, we have determined that such a convolution eliminates the spikiness introduced by simple differencing and, therefore, is the preferred method for differentiation in the calculations presented in this paper.

We have carried out experiments to determine the grid size required to produce a smooth seismogram. As an example we show, in figure 4, the variation of the waveform and maximum amplitude of a seismogram as a function of grid size for a sample reflection problem. The reflecting flat surface is specified for seismograms A, B, and C by grid areas of a wavelength of 4 km. Hence for seismograms A, B, and C the number of grids per wavelength is 11.4, 8 and 4 respectively. Seismogram C shows that the coarse discrimination of the surface has introduced high frequency noise which degenerates the waveform and the maximum amplitude. For each problem we calculate, the grid size is selected by trial and error. The grid is made progressively finer until the solution is unvarying as shown in figure 4.

Applications

The development of any numerical procedure necessitates a comparison with known exact solutions. To see that the integral is being calculated correctly, the results of this code are compared with an analytical formula developed by Hilterman (1975). For the source and the receiver together above an arbitrary rigid surface, Hilterman reduces the Kirchhoff integral to the following form:

$$u_r(\underline{r},t) = \frac{1}{2\pi c}\left[\left(f(t) * \frac{2}{t}\frac{d\Omega}{dt}\right) + \left(\frac{df}{dt} * \frac{d\Omega}{dt}\right)\right] \tag{15}$$

Here * denotes convolution. $\frac{d\Omega}{dt}$ is the increase of solid angle with a vertex at the source-receiver point subtended by the surface as a function of time (Hilterman, 1975). We choose to calculate the response to a point source in a fluid overlying a rigid hemisphere imbedded in a infinite rigid plane. (see Fig. 5 for the geometry) For such a geometry we have determined $\frac{d\Omega}{dt}$ to be

$$\frac{d\Omega}{dt} = \frac{\pi}{|\underline{R}|}\left\{\frac{2(|\underline{R}|^2 - a^2)}{ct^2} - \frac{c}{2}\right\} H(t - \tau_0) \text{ for } \tau_0 \le t < \tau_1 \tag{16}$$

$$\frac{d\Omega}{dt} = \frac{2\pi\tau_0}{t^2} H(t - \tau_1) \qquad \text{for } \tau_1 \le t \tag{17}$$

where $\tau_0 = 2(|\underline{R}| - a)/c$, the minimum two-way travel time, and $\tau_1 = 2(|\underline{R}|^2 + a^2)^{1/2}/c$. $H(t)$ is the assumed source time function and is the unit step function. Using these results, we calculate the following two terms ϕ_A and ϕ_B analytically and numerically to check on the accuracy of the integral approximation.

$$\phi_A = \frac{1}{2\pi c} H(t) * \frac{2}{t}\frac{d\Omega}{dt} \tag{18}$$

$$\phi_B = \frac{1}{2\pi c} \int_{\tau_0}^{t} \frac{dH}{d\tau} * \frac{d\Omega}{d\tau} d\tau \tag{19}$$

The comparison is shown in Figure 5. In this calculation, the source-receiver point is 20 km above the center of the hemisphere with a radius of 5 km. The velocity of the medium is 6 km/sec. The agreement is good for τ_0 + 15 seconds. The results differ because the integral is calculated numerically over a finite surface. The conclusion from this experiment is that the numerical evaluation of the integral is adequate.

We further test the code by comparing the Kirchhoff solutions with analytical high frequency solutions which satisfy the given boundary conditions. Again we choose to calculate the potentials caused by a point source impinging on a rigid sphere; however we allow the source and receiver to separate. The Kirchhoff results are compared to those from a first motion approximation of an aymptotic form of a solution obtained by Gilbert and Helmberger (1972). They solve the problem of the reflection of an SH pulse from a fixed and rigid sphere. Figure 6 illustrates the geometry and parameters used in this problem. The displacement as a function of spherical polar coordinates (r,θ) obeys the following equation.

$$\mu\nabla^2 u(r,\theta,t)-\rho\frac{\partial^2 u}{\partial t^2}(r,\theta,t) = \frac{-f(t)\delta(r-r_0)\delta(\theta-0^+)}{2\pi r^2\sin\theta} \tag{20}$$

Here μ is the rigidity of the medium, ρ is the density, and c is the wavespeed ($c=\sqrt{\mu/\rho}$). The Gilbert and Helmberger asymptotic solution for the reflected pulse is

$$\bar{u}_r = \frac{-f(s)s^{\frac{1}{2}}}{2\pi\mu(2\pi rr_0\sin\theta)^{\frac{1}{2}}} \, Im \int_C^{C+i\infty} \frac{\gamma^{\frac{1}{2}}\exp(-s(\gamma\theta+\Psi))d\gamma}{\left(\frac{r_0^2}{c^2}-\gamma^2\right)^{\frac{1}{4}}\left(\frac{r^2}{c^2}-\gamma^2\right)^{\frac{1}{4}}} \tag{21}$$

$\bar{u}_r$, f(s) are the Laplace transform of u(r,θ,t) and f(t). The variables γ and ψ and the path of integration are defined in Gilbert and Helmberger (1972). After performing the first motion approximation we obtain for the reflected pulse

$$u_r = -\frac{1}{4\pi\mu} \left[\frac{a(\cos i)(\sin\rho)}{\sin\theta r_o(R_o r\cos\rho + R r_o\cos\rho_o)}\right]^{\frac{1}{2}} f\left(t - \left(\frac{R_o+R}{C}\right)\right) \tag{22}$$

and for the direct pulse

$$u_d = \frac{1}{4\pi\mu} \ f\left(t - \frac{R'}{c}\right)/R' \tag{23}$$

where R′ is the distance between the source and the receiver.

If the source and receiver are together, it can be shown that solution (22) and a far-field first motion approximation to the Kirchhoff solution are equivalent. First let us define a geometric spreading factor S such that equation (22) may be rewritten as

$$4\pi\mu \ u_r = -S \ f\left(t - \left(R_o + R\right)/c\right) \tag{24}$$

Now we examine the Kirchhoff solution when the source and receiver are together. Following an approach developed by Hilterman the first term in equation (15) is discarded as a near-field term.

$$4\pi\mu \ u_r(\underline{r},t) = -\frac{1}{2\pi c} \left\{\frac{\partial f}{\partial t} * \frac{d\Omega}{dt}\right\} \tag{25}$$

Then a first motion approximation is made.

$$\frac{d\Omega}{dt} * \frac{d\Omega}{d\tau}\bigg|_{t=\tau_o} H(t - \tau_o) \tag{26}$$

Then

$$4\pi\mu \; u_r(\underline{r},t) \; = \; - \; \frac{d\Omega}{dt} \; \Bigg|_{t=\tau_o} \; f(t - \tau_o) \tag{27}$$

From equation (16) we find that

$$4\tau\mu \; u_r(\underline{r},t) \; = \; - \; \frac{a}{2(R_o + a)R_o} \; f(t - \tau_o) \tag{28}$$

If we now take the limiting value of S as $R \to R_o$ and $\theta \to 0$ in equation (22), the result is

$$S \; = \; \frac{a}{2(R_o + a)R_o} \tag{29}$$

Hence, the two far-field high frequency solutions are formally equivalent when the source and receiver are together. A similar result is obtained by Hilterman (1975) for a rigid planar surface.

The Kirchhoff solutions are also calculated when the source and receiver are separated and the maximum amplitudes of the synthetics are compared with those amplitudes predicted by equation (22). The time history of the input source for this problem is described by the third derivative of equation (14) with the overshoot constant $B = 2$ and $k = 10$. The medium has a shear wave velocity of 5 km/sec; thus the wavelength of the input source is approximately 4 km. The gridlength used in these calculations is .1 km, making the number of grids per wavelength equal to 40. The total grid area needed to describe the surface of the sphere is 400 km^2. The gridlength was selected to give

an extremely fine sampling of the surface so that we may investigate the effects of a wide range of pulse widths as input time histories. Six ramp responses for this problem required 595.8 seconds of CPU time on a PRIME750. Table 1 shows the parameters used in th   numerical experiments and the numerical and theoretical amplitudes. The results compare favorably; the accuracy of the Kirchhoff solutions is better than or equal to 1 %.

The above two experiments indicate that the Kirchhoff code correctly predicts reflections from curved surfaces with large reflection coefficients and far-field receivers. Similiar efforts have been carried out by workers in the field of electromagnetic scattering. Jiracek (1972) computes the amplitudes of electromagnetic waves caused by an incident transverse electric plane wave impinging on a perfectly conducting two-dimensional sinusoidal surface. He compares results obtained from a Rayleigh-FFT method, an integral equation solver, and the Kirchhoff method. The most obvious failure of the Kirchhoff technique to predict correct amplitudes occurs when the incident angle is past critical angle. This result is not surprising in light of assumptions made in estimating the boundary values on the surface. However, for angles less than critical, the Kirchhoff code is adequate and inexpensive for problems involving three-dimensional rough surfaces.

We can gain further insight into the usefulness of this formalism by comparison of the Kirchhoff solutions with optical solutions to problems of geophysical interest. First, the technique is applied to the calculation of reflections from a mountain with a buried source. In the second application, reflections from a plane where the reflection

coefficient varies as a function of position on the surface are computed. In both calculations, particular attention will be paid to those propagation paths where classical ray theory fails.

The first application of the code is the calculation of the reflected potentials from an isotropic source underneath an idealized mountain (see Fig. 7). The topography of the mountain is calculated from this formula where Z is the height of the surface.

$$Z = \frac{C}{2}\left(1 - \cos\left(\frac{2\pi}{W}\left((x^2 + y^2)^{\frac{1}{2}} - \frac{W}{2}\right)\right)\right) \tag{30}$$

Here C, the maximum height, is 5 km, and W, the width, is 33.33 km. The acoustic reflection coefficient is −1 everywhere on the surface. The topography is specified on 150 x 150 km grid with each element of the grid being .5 km long.

Since the angle between the normal of the surface and the incident source ray is calculated by the code, it is simple to plot the path of the reflected rays. These rays are traced for two depths below the baseline of the free surface. In the first plot, Figure 7, we can see the rays from a source at 10 km which reflect off the free surface and travel to a depth of 50 km. This figure shows the position of the ray caustic, focii, and the shadow zone caused by the convex shape of the mountain. These features will influence the waveforms considerably.

In Figure 8 the rays are traced to a depth of 1000 km. The Kirchhoff responses are calculated at this depth at the marked positions which vary from 0 kilometers to 750 kilometers horizontally. Upon closer inspection of Figure 9, one can see slight asymmetries in the

location of the rays with respect to the position at 0 kilometers.
These asymmetries are caused by the discretization of the surface of the
mountain. The error in the value of the computed normal derivatives
introduces   10 km of uncertainty into the location of the rays at this
depth.

The calculated reflected responses are shown in Figure 9.   These
pulses are convolutions of the ramp response with the Haskell function
with the parameter B=0 and k=25.   Hence the number of grids per
wavelength is 10.   As the horizontal distance of the receiver changes,
we see systematic waveform variations which can be interpreted in terms
of rays interacting with caustics.   In the ranges of 0, 50, 100, and 150
kilometers the synthetics have complicated pulse shapes caused by the
interference of three families of rays. The first arrival is a simple
pulse with a π phase-shift which is a consequence of the reflection off
the free surface. The second pulse is a reflected ray with a path which
is tangent to the caustic formed by the mountain. This path results in
a π + π/2 phase-shift of the pulse. The third arrival reflects off the
mountain and travels through the geometric focus caused by the mountain;
thus the phase shift of this arrival is π + π . The maximum amplitude
of these four distances is controlled by the interference of these rays.
Clearly the high amplitude and the simple pulse of the first synthetic
at 0 kilometers is a result of the constructive interference of the
first two rays.   Past 150 kilometers, the latter two arrivals arrive
closely in time and their interference controls the amplitude and
frequency content of the second pulse on the record. From Figure 8 , it
is clear that a ray interpretation of pulses on records past 400

kilometers is no longer valid. Ray theory predicts only one reflected pulse because the mountain creates a shadow zone; yet one sees two distinct pulses predicted by the Kirchhoff method. The second phase-shifted pulse decreases in amplitude and frequency content. As the horizontal distance of the receivers increases, the amplitude of the first reflection becomes the maximum amplitude of the record. If one calculates the maximum amplitudes of reflections off a plane for the same source- receiver geometry, one can see that the two sets of amplitudes merge. This behavior is shown in Figure 10 where the amplitudes as a function of horizontal distance for the two geometries have been calculated. The solid line shows the decay of amplitudes calculated for a planar surface. The triangles are amplitudes calculated for a mountain with a height of 2 kilometers and a width of 10 kilometers. The two sets of values coincide past 800 kilometers.

The Kirchhoff results for this experiment are gratifying because one does not expect infinite amplitudes or abrupt shadow zones predicted by optics in real physical systems. This experiment also demonstrates that this technique produces the requisite phase shifts in an extremely simple manner unlike existing ray tracing techniques which must track the behavior of a ray tube along the propagation path.

The second application of the code is the calculation of reflections off an acoustic planar free surface where the reflection coefficients are allowed to vary as a function of position on the surface. These calculations demonstrate the flexibility of the code and again emphasize the differences between the Kirchhoff solution and optics. (The wavespeed of the medium is 6km/sec for all the following

calculations).

Initially one assumes that the reflection coefficient is zero for elements of the plane within a circular aperture of radius R and is -1 for elements outside this aperture. The source is directly underneath the center of the hole. From ray theory one expects that no reflected energy will arrive at a receiver directly underneath the source. Yet one calculates non-zero amplitudes for both long and short period WWSSN seismograms from the Kirchhoff code. These seismograms are displayed in Figure 11 as a function of the radius of the aperture for a receiver 1000 kilometers below the surface. Only the reflected pP phase has been calculated and convolved with WWSSN instruments.

This pulse is systematically delayed as the radius of the hole increases from 1 to 5 kilometers. There is no change in the waveforms. Only the amplitudes of both sets of seismograms decrease. However the amplitude of the seismograms for an aperture with a five kilometer radius is more than half the magnitude of the amplitude of a pP phase reflected from a free surface without a hole. Clearly, then, ray theory is not a good approximation to the solution to this problem.

In addition, ray theory fails to predict any dependence of the reflected amplitudes on frequency. Intuitively one expects, for an aperture problem, that the higher frequencies of a broad-band signal will be reduced relative to the lower frequencies after reflection. This hypothesis is tested by calculating the reflected responses from sources of differing frequency content. In the following calculations the parameter B of the modified Haskell source representation equals zero; however k varies from 5 to 25. An increase in k broadens the

bandwidth of the incident signal (von Seggern and Blandford, 1972). One computes two responses for a given source pulse. The first response is a reflection off the plane with a hole and the second is a reflection off the plane without a hole. The amplitude of the latter response has no frequency dependence; hence if the reflection from a hole has no frequency dependence, one predicts that the ratio of the amplitudes of the two reflections will be constant as a function of the parameter K. However, if there is a frequency dependence, the ratios should vary systematically.

From numerical experiments one confirms the frequency dependence of the reflected amplitudes. This result is shown in Figure 12. Specifically, the amplitudes of the reflections from the aperture are always smaller than the amplitudes of planar reflections. Also the ratio of the two responses decreases when B decreases if the receiver is located at position 2. This behavior is displayed for apertures with three radii, 2, 3, and 4 km.

However, this behavior does not occur if the receiver is located at position 1, 1000 km directly below the source. The ratios are approximately constant as B decreases. This observation suggests that, here, the reflected amplitudes from the aperture do not depend on the bandwidth of the signal. Although this result is not intuitive, it is typical of analytical solutions to Fraunhofer diffraction from apertures in an opaque screen (Born and Wolf, 1964). For example, the solution of the intensity of light transmitted through a rectangular aperture has the functional form of

$$\frac{\sin(A\omega x)}{A\omega x} \cdot \frac{\sin(B\omega y)}{B\omega y} \tag{31}$$

where A and B are geometric constants and x and y are the rectangular coordinates of the position of the receiver. The limit of the above function as x and y approach zero is 1 and is independent of the value of ω.

Such experiments, which vary the reflection coefficients on the free surface, may be applicable to the analysis of the effects of spallation generated by nuclear blasts on teleseismic P-wave reflections. Spall is the physical separation of near surface layers during the explosion. Material above the bomb is either ejected or returns to produce an impact signal on near-field instruments. This non-linear and non-elastic behavior of the material surrounding the source may result in amplitude and travel time anomalies of reflected sP and pP phases.

The model used to simulate spall is one where the reflection coefficient is a cosine taper; that is

$$R = \left(\cos\left(\frac{\pi x}{2R}\right) - 1\right) \qquad x \leq R \qquad (32)$$

$$R = -1 \qquad x > R \qquad (33)$$

Here x is distance from the source epicenter on the free surface. One chooses this behavior of the reflection coefficient to simulate material reflecting more energy as the distance from the source increases. The model introduces complications into the short period waveforms but only broadens the long period waveforms. This effect and the source-receiver geometry is illustrated in Figure 13. The geometry is the same as used in the aperture calculations. Unlike the first model, this model causes the amplitudes of both the long and short period reflections to decay

quite rapidly. The amplitude decay is greater for the short period reflections than for the long period reflections. Hence the long period energy is insensitive to the perturbation of the reflection coefficients relative to the short period energy.

The source-receiver geometry is changed for this particular model to test the hypothesis that asymmetries of spalling with respect to the source location can introduce observable azimuthal variations of amplitudes and waveforms of teleseismic records of nuclear blasts. Such variations have been documented for teleseismic recordings of Nevada Test Site blasts (Helmberger and Hadley, 1981). In addition, photographs of collapse craters from NTS blasts suggest that processes like spalling and subsidence occur along pre-existing planes of weakness which are not symmetrical with respect to the emplacement hole (Springer and Kinnaman, 1971). Figure 14 shows the results for stations at three azimuths. The source is placed 2 kilometers to the right of the center of the spall aperture and 1 kilometer below the free surface. The receivers are all at horizontal distance which corresponds to a take-off angle of 20° for the direct P wave. One sees azimuthal variations of waveform and amplitudes for both long and short period reflections. The amplitude variations are not large but the waveform changes are dramatic for short period records.

This model is crude and consequently does not demonstrate that spalling affects teleseismic reflections. However, Shumway and Blandford (1980) report observing a systematic delay in arrival times of pP phases from explosions. The simple aperture experiment provides an explanation for that delay. In addition the Kirchhoff technique allows

one to specifiy more realistic dynamical information on the free surface and calculate more realistic models in a straightforward manner.

Conclusions

A numerical procedure has been presented for the evaluation of the Kirchhoff- Helmholtz integral assuming the tangent plane hypothesis. The method is a high frequency one and produces results which compare well with existing asymptotic first motion solutions. The technique has been applied to two problems and compared to classical ray theory results. First, the reflections off an idealized mountain are calculated and have phase-shifts consistent with those predicted by optics; however, the amplitudes at triplications are finite unlike the classical ray result. In addition diffracted pulses are produced in the shadow zones. The second application is the calculation of reflections where the reflection coefficients vary as a function of position. For a hole in the free surface, the Kirchhoff method produces reflections where ray theory predicts no reflections. The method also produces amplitudes which are frequency dependent. The results are applied and extended to model the effects of spallation on teleseismic reflections. Travel time delays and amplitude anomalies are predicted. These anomalies are consistent with observations although the observations are not modeled.

In conclusion, the method has a broad range of applications. The method is inexpensive to run for modeling two and three dimensional rough surfaces. Although the method is appropriate for narrow angles of reflections and acoustic reflections, its range of applicability can be extended by introducing new time functions on the boundary. The code

can also be coupled with existing propagational techniques such as ray-tracing, Cagniard-de Hoop methods, or full wave theory. This coupling will enable one to handle more complicated and relevant seismological problems.

ACKNOWLEDGEMENTS

REFERENCES

Aki and Larner, 1970. Surface motion of a layered medium having an irregular interface due to incident plane SH waves, J. Geophys. Res., 75, 933-954

Berryhill,J.R., 1977. Diffraction Response for Nonzero Separation of Source and Receiver, Geophys., 42, 1158-1176

Boore, D.M.,K.L. Larner, and K. Aki, 1971. Comparison of two Independent Methods for the Solution of Wave Scattering Problems: Response of a Sedimentary Basin to Vertically Incident SH waves, J. Geophys. Res., 76, 588-569

Born, M. and E. Wolf, Principles of Optics, The MacMillan Co., New York, 1964.

Cole, David, A numerical boundary integral equation method for transient motions, Thesis, California Institute of Technology, 1980.

Davies, H., 1954. The reflection of electromagnetic waves from a rough surface , Proc. Inst. Elec. Eng., Vol. 101, pt. 4, 209-214

Gilbert and Helmberger, 1972. Generalised ray theory for a layered sphere, Geophys. J. R. Astr. Soc., 27, 57-80

Glover and Alexander, 1969. Lateral variations in crustal structure beneath Montana LASA, J. Geophys. Res., 74, 505-531

Hilterman, F.J., 1970. Three-dimensional seismic modeling, Geophys., 35, 1020-1037

Hilterman, F.J., 1975. Amplitudes of seismic waves - a quick look, Geophys., 40, 745-762

Hong and Helmberger, 1978. Glorified Optics and Wave Propagation in Non-Planar structure, B.S.S.A., 68, 1313-1330

Jiracek, George, Geophysical studies of electromagnetic scattering from rough surfaces and from irregularly layered structures, Thesis University of California at Berkeley, 1972.

Mitzner, K.M., 1967. Numerical solution for transient scattering from a hard surface of arbitrary shape - retarded potential technique, J. Acoust. Soc. Am., 42, 391-397

Mow, Chao-Chow and Yih-Hsing Pao, The Diffraction of Elastic Waves and Dynamic Stress Concentrations, #R-482-PR , A report prepared for United States Air Force Project Rand, 1971.

Shumway and Blanford, 1980. On detecting and estimating multiple arrivals from underground nuclear explosions, Earthquake Notes, 50, no. 4, p. 34

Smith, Warwick D., 1975. The application of finite element analysis to body wave propagation problems, Geophys. J. R. Astr. Soc., 42, 747-768

Springer and Kinnaman, 1971. Seismic Source Summary for U.S. Underground Nuclear Explosions, 1961-1970, B.S.S.A., 61, 1073-1098

Trorey, A.W., 1970. A simple theory for seismic diffractions, Geophys., 35, 762-784

Trorey, A.W., 1977. Diffractions for arbitrary source-receiver locations, Geophys.,42, 1177-1182

von Seggern, D. and R. Blandford, 1972. Source time functions and spectra for underground nuclear explosions, Geophys. J., 31, 823-897

Walck, M.C. and J.B. Minster, 1980. Relative array diagram scanning of crust and upper mantle, Southern California, EOS, _61_, p. 300

FIGURE CAPTIONS

1. The discretization of the surface over which the Kirchhoff integral is calculated.

2. The closed surface of integration which is composed of S_α the surface over which one carries out the numerical integration, and S_β , the remainder which does not contribute to the signal in the time window of interest.

3. The summation of the response from each element to obtain the total response.

4. This figure shows the change of response as the element size in creases. The model used here is a free surface with a hole. The source and receiver are directly below this hole. The response is convolved with a modified Haskell source and a short period WWSSN instrument to produce the above seismograms.

5. The geometry of the point source problem is shown at the top of figure. Here a is the radius of the hemisphere. $\underline{r}$ is the vector from the source-receiver point to an arbitrary position on the surface. $\underline{R}$ is the vector extending from the center of the hemisphere to the source-receiver point. Below are the two parts of the solution ϕ_A and ϕ_B. The dotted lines are the values computed by the numerical integration. The solid lines are the values computed by the analytical Hilterman solution.

6. Geometry of the spherical problem.

7. The rays which reflect off a mountain described by the equation (30). The source is 10 km below the baseline indicated by the dashed line. Also shown are the caustics formed by such a mountain and the geometric focus.

8. The rays which reflect off the mountain are traced to a depth of 1000 km.

9. The responses convolved with a modified Haskell source for receivers all at a depth of 1000 km and at horizontal distances which vary from 0 to 750 km away from the center position.

10. The maximum amplitude of the waveforms calculated for two free surfaces is shown as a function of horizontal distance away from the center. The receivers are at a depth of 1000 km. The solid line is the value of the maximum amplitude of reflections off a plane from a source 10 km below the free surface. The triangles are values for a free surface with a mountain of height 2 km and width 10 km for the same source-receiver geometry.

11. Long (dashed lines) and short (solid lines) period WWSSN seismograms calculated for the geometry shown at the top of the figure. Here the radius of the hole varies from 1 to 5 km.

12. Ratio of maximum amplitude of reflection from a surface with and without a hole. The open circles are ratios measured at a receiver directly underneath the source and the center of

the aperture. The triangles are ratios measured at a receiver 68 km away from the center position. Both receivers are 1000 km be low the free surface. The radius of the hole R is 2,3, and 4 km. The ratios are plotted for these radii as a function of k. (a measure of the bandwidth)

13. Long and short period seismograms for a cosine tapered reflection coefficient.

14. Long and short period seismograms from receivers located at positions A , B, and C.

Parameters used in calculation of Response from a Sphere with radius a= I0km

R km	R$_0$ km	i (°)	reflected amplitude (Kirchhoff)	reflected amplitude (theoretical)
90.6	90.6	6.3	.024040	.02467
92.2	92.2	12.5	.02320	.02383
94.9	94.9	18.4	.02202	.02257
42.3	95.2	18.9	.04567	.04667
17.5	105.2	31.0	.07967	.08218
55.9	55.9	26.5	.08914	.09163
128.1	128.1	38.6	.01228	.012667
62.5	62.5	36.8	.0725	.074607

Fig. 1

Fig. 2

Fig. 3

Fig. 4

Fig. 5

Fig. 6

33.33 km
5 km
15 km
Caustic
Source focus
Geometric focus

0 10 20 30 40
km

Fig. 7

200 km

200 km

Fig. 8

Fig. 9

Horizontal Distance (km)

Max. ampl. (×10⁻²)
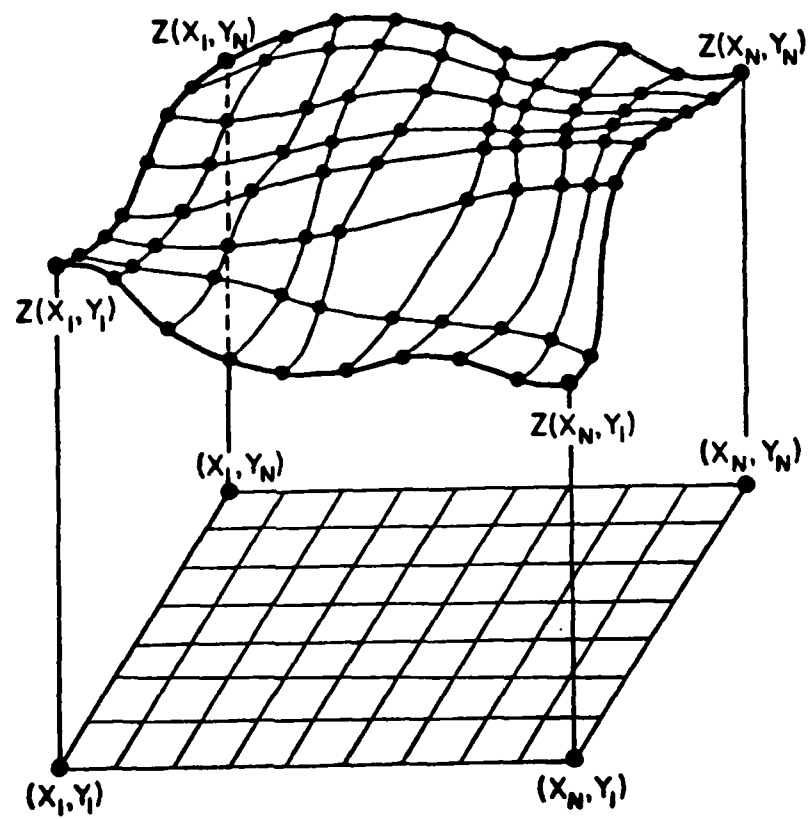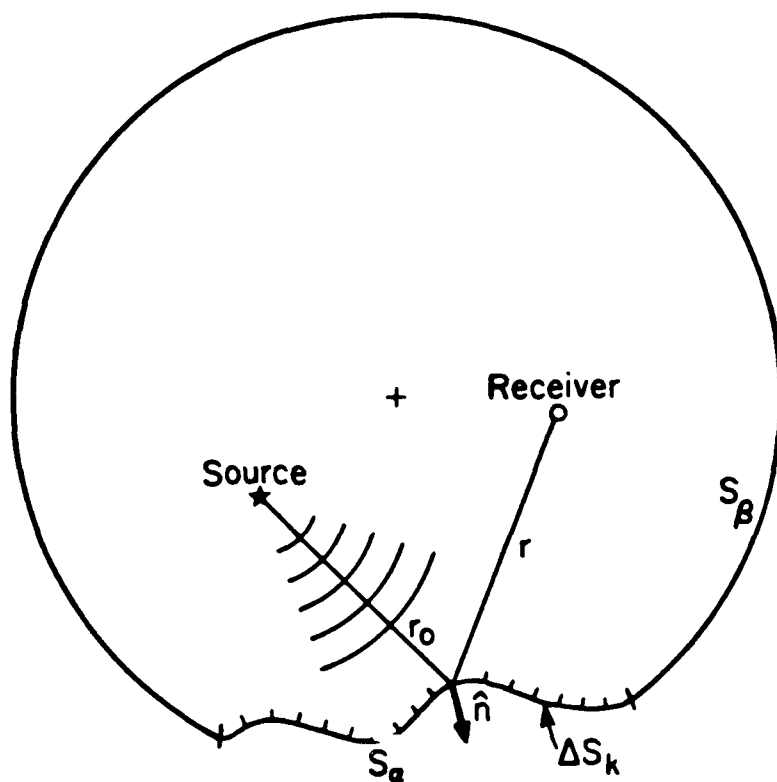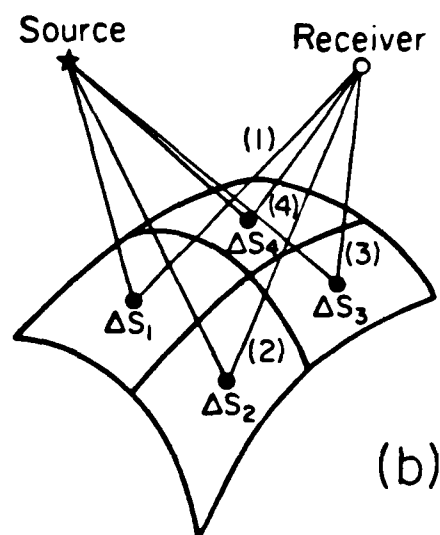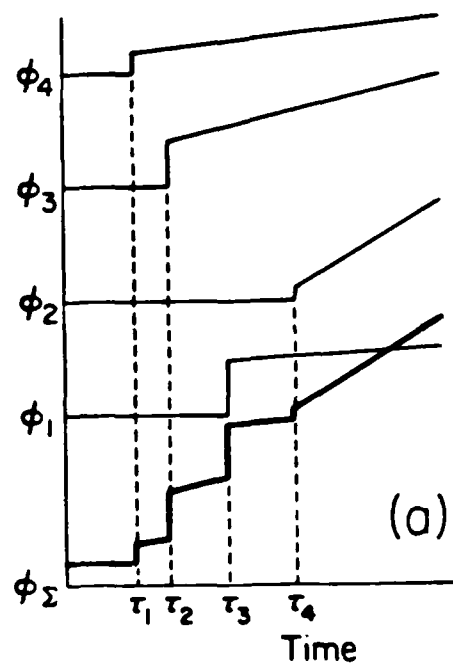
Fig. 10

Fig. 11

Fig. 12

Fig. 13

$x \leq R$: Refl. Coeff. $= \cos\left(\dfrac{\pi x}{2R}\right) - 1$

$x > R$: Refl. Coeff. $= -1$

Radius = 4 km

$\Delta S_K = 0.25$ km^2

1000 km

Source

$\theta = 20°$

Vel. = 6 km/sec

A   B   C

WWSSN SYNTHETICS

S.P.
L.P.

A $L = 0.255 \times 10^{-2}$
     $S = 0.128 \times 10^{-1}$

B $L = 0.298 \times 10^{-2}$
     $S = 0.161 \times 10^{-1}$

1 sec

C $L = 0.227 \times 10^{-2}$
     $S = 0.920 \times 10^{-2}$

Fig. 14